High-T_c Superconductive Wideband Compressive Receivers

W. Gregory Lyons, Duane R. Arsenault, Alfredo C. Anderson, T.C.L. Gerhard Sollner, Peter G. Murphy, Mark M. Seaver, Rene R. Boisvert, Richard L. Slattery, and Richard W. Ralston

Wideband compressive receivers are an attractive application of analog high-transition temperature superconductive (HTS) microwave filters. Chirp filters form the basis of compressive receivers, implementing a chirp-transform algorithm in the analog domain for real-time spectral analysis. HTS tapped-delay-line chirp filters are an enabling technology for instantaneous bandwidths greater than 1 GHz, and have evolved sufficiently to support dispersive delays as long as 40 nsec with multigigahertz bandwidths and time-bandwidth products in excess of 100. Long dispersive delays have been obtained by using a bonded/thinned-wafer technique to fabricate $YBa_2Cu_3O_{7-\delta}$ stripline devices on 5-mil-thick, 2-in-diameter $LaAlO_3$ substrates. These filters have produced better than –18-dB error sidelobes. In addition, a 3-GHz-bandwidth HTS compressive cueing receiver was recently delivered to the Naval Research Laboratory to be flown on the High-Temperature Superconductivity Space Experiment (HTSSE), and demonstrations have been performed by combining HTS chirp filters with conventional compressive-receiver hardware. We propose a novel compressive cryoreceiver architecture that combines HTS, cryoelectronic, and advanced high-speed semiconductor technologies. The proposed receiver will rival the sensitivity of a narrowband receiver while providing unprecedented instantaneous wideband frequency coverage, and future developments will extend the bandwidth capability. We make detailed comparisons to an all-digital receiver and to channelized-filter receiver architectures. An HTS compressive receiver is projected to be superior in overall size, weight, and power; its applications include electronic warfare and dynamic molecular spectroscopy for remote sensing.

Tremendous progress has been made since 1986 in the application of thin-film high-transition temperature (high-T_c) superconductors to passive analog microwave devices [1–3]. High-quality, high-T_c superconductive (HTS) thin films with microwave surface resistances many orders of magnitude below that of copper at 77 K can now be reliably deposited over a 3-in-diameter substrate area. This advance has led to the implementation of a large variety of HTS passive microwave device structures. The planar nature of thin-film HTS structures offers a substantial size and weight advantage over low-loss waveguide structures made from normal metal, and the cryogenic operation of HTS devices affords the system engineer an opportunity to achieve a very low-noise receiver front end. Planar HTS struc-

tures require two-dimensional lithographic techniques to define devices rather than tedious and inaccurate three-dimensional machining techniques that waveguides and dielectrics typically require. Careful design of HTS microwave devices in conjunction with low-loss dielectrics at cryogenic temperatures may also allow higher quality factors (Q) and lower losses to be obtained than with conventional waveguide structures.

Passive microwave devices were an early favorite in the history of HTS thin-film development efforts because of their simple single-layer structure. Researchers soon learned, however, that a very low-loss passive microwave device depends on HTS film quality and design techniques to the same extent as an active multilayer Josephson-junction circuit. For example, we understand that a high-Q HTS microwave device with good power-handling capability requires roughly the same film quality as a low-noise two-junction HTS circuit for magnetic sensing [4]. Good-quality HTS films can be readily obtained today and a variety of useful HTS microwave device structures has been demonstrated. Researchers are now focusing on filter structures and HTS applications that will have the greatest impact on their respective overall microwave system (e.g., radar system, communications satellite, or remote-sensing receiver).

This enhancement in system-level performance must be significant enough to justify the burdens of cryogenic cooling, which include increased power consumption, increased size and weight, and potentially reduced reliability. The 4.2-K operating temperature of conventional superconducting microwave devices severely limited their application because the cryogenic systems required to achieve 4.2 K are too complex and cumbersome. The advent of HTS devices eases this cryogenic burden. Operating temperatures between 50 and 90 K allow the use of simpler, smaller, more reliable, and less power-hungry cryogenic coolers, such as those used or planned for infrared-imaging systems on remote-sensing satellites and military platforms [5].

HTS chirp filters are an important example of a passive microwave device that has a significant system-level impact. They represent an enabling technology because they support bandwidths beyond the 1-GHz limit of surface-acoustic wave (SAW) compressive receiver technology [6] and the 2-GHz limit of acousto-optic channelizer technology [7], and because superconductivity is the only technology that successfully supports multigigahertz bandwidths in an accurate chirp-filter structure [8, 9].

The chirp filter and analog chirp-transform algorithm form the basis of a spectral-analysis receiver known as a compressive receiver. The term "compressive receiver" is derived from the receiver's use of an analog Fourier transform to perform a virtual channelization of the wideband input and compress each RF input tone into a narrow pulse. The detected output from a compressive receiver consists of these narrow, or compressed, pulses, each representing the frequency bin of a transformed input signal, arriving in sequential order in the time domain. The input frequency of the signals is determined by measuring the time positions of these pulses. Since the detected pulses can appear close together in time and because they are extremely narrow (the pulsewidth is inversely proportional to the analysis bandwidth), high-speed logic circuits are required to process the pulses. The HTS wideband compressive receivers described in this article and in Reference 10 represent a union between a multigigahertz-bandwidth HTS-based analog chirp transform and advanced high-speed semiconductor circuits for pulse processing.

The virtual channelization function of a compressive receiver is power efficient, and provides the fine frequency resolution and sensitivity normally available only from a narrowband receiver. These attributes are desirable in military electronic-warfare applications and in dynamic molecular spectroscopy for remote sensing. Both applications demand extremely wide bandwidth coverage, constantly pushing the state of the art in receivers. Military electronic-warfare applications push toward continuous time coverage of tens of gigahertz of bandwidth with the highest possible dynamic range and sensitivity. Remote-sensing applications, such as satellite-based dynamic molecular spectroscopy of the atmosphere, often involve multigigahertz-wide molecular-excitation linewidths. The compressive receiver's ability to simultaneously measure the full extent of these broad linewidths leads to greatly reduced integration times.

Furthermore, the HTS wideband compressive receiver has size, weight, and power advantages over conventional technology. By delivering improved performance over a wider bandwidth and in a more compact design, the HTS wideband compressive receiver can meet the demands of existing applications.

Superconductive Chirp Filters

Chirp filters, which have been used extensively in pulse-compression radars, are the backbone of a compressive receiver. These filters are also known as dispersive delay lines and linearly frequency-modulated delay lines. Early chirp filters were made with folded-tape meanderlines or crimped coaxial cable. Folded-tape meanderlines produced a phase shift in each turn of the meander, with the phase shift dependent on the turn-to-turn coupling. A meanderline was meticulously synthesized by manipulating the number of sections, and for each section, manipulating the center frequency, the number of turns, and the turn-to-turn coupling. The crimped coaxial cable used backward reflections created by impedance discontinuities at each crimp to provide the chirp filtering [8].

The acceptance of chirp filters as a system component did not occur until accurate and large time-bandwidth-product SAW chirp filters were developed. A wide variety of effects, however, limit the bandwidth of SAW chirp filters, including propagation loss, transducer inefficiency, and difficulty in fabricating the submicron dimensions required by high-frequency transducers. Attempts have been made to build chirp devices with magnetostatic wave (MSW) media, but the tremendous dispersion in MSW materials makes this strategy impractical [7]. For other chirp devices, such as folded-tape meanderlines and crimped coaxial cable, insertion loss and the device accuracy limit system applications.

The concept of a superconductive chirp filter was initially proposed by J.T. Lynch, and subsequently reduced to practice and patented by a Lincoln Laboratory research team [11, 12]. This work grew out of an effort by S.A. Reible to build superconductive analog convolver structures in the gigahertz range, which paralleled research at the time into SAW-based devices [13]. The two advantages of superconductors in transmission-line structures are their extremely low loss at microwave frequencies and their nondispersive (i.e., frequency independent) penetration depth. These advantages lead to long and compact electromagnetic delay lines. Introducing filter taps into these delay lines can produce a superconductive chirp filter that extends the bandwidth capability of chirp filters beyond the 1-GHz limitation of SAW devices.

A chirp filter is a form of a fixed tap-weight transversal filter, which is a general class of filters used to implement matched filtering, correlation, convolution, and Fourier transformation. Figure 1 illustrates the generalized transversal-filter structure. Filter taps provide samples of the input signal differentially delayed in time by an amount τ_i. These time-delayed

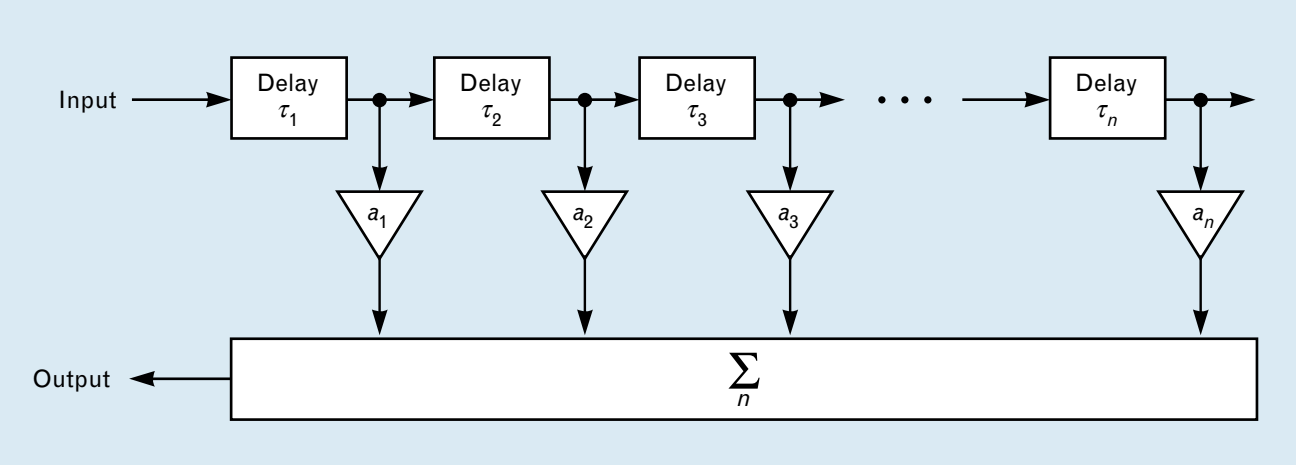

FIGURE 1. Generalized transversal-filter structure with time delays τ_i and tap weights a_i. Time-delayed samples of the input signal are amplitude weighted by the appropriate a_i and coherently summed to produce the filter output.

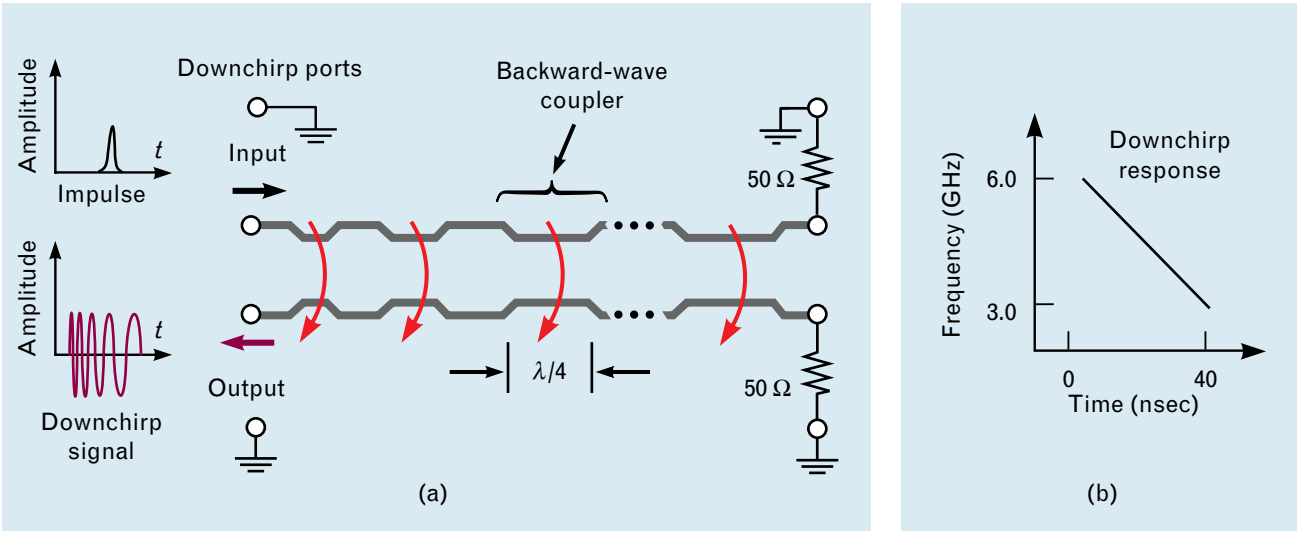

FIGURE 2. (a) Structure and operation of a proximity-tapped superconductive chirp filter. The upchirp ports have been terminated into 50 Ω. The electromagnetic delay lines are implemented in stripline and the taps are implemented by a cascade of backward-wave couplers. (b) The downchirp impulse response is shown for a typical 3-GHz-bandwidth, 40-nsec-long chirp filter.

samples are amplitude weighted by a factor a_i and coherently summed to produce the filter output. The number of information cycles of the waveform gathered coherently in the filter determines the signal processing gain, measured conveniently as the time-bandwidth product.

Figure 2 illustrates the operation of a proximity-tapped superconductive chirp filter [14, 15]. The transmission-line structure is typically stripline, and upper and lower ground planes sandwich the signal lines. This structure usually involves two substrates with signal lines and lower ground plane on opposite sides of the bottom substrate, and the upper ground plane on the top side of the top substrate. For clarity, Figure 2(a) shows only the signal lines. A series of backward-wave couplers achieves the downchirp filter response (group delay increases as frequency decreases) in direct analogy to a SAW chirp grating or transducer array. Each coupler has a peak response at the frequency for which the coupler is a quarter-wavelength long. Making the reciprocal of the length of each coupler a linear function of the length along the line causes the peak frequency response of the backward-wave couplers to vary as a linear function of delay. Weighting of the taps is achieved by varying the coupling strength between the two striplines forming each backward-wave coupler. Line-to-line isolation greater than about –55 dB must be maintained in the uncoupled sections of the filter.

Figure 2(b) illustrates the downchirp operation of a superconductive chirp filter over a typical 3-GHz bandwidth with a dispersive delay of 40 nsec. The device is symmetric and is operated by using either its downchirp or upchirp ports. An impulse function applied to the downchirp ports produces a downchirp signal over the bandwidth of the chirp filter, as shown. The 6.0-GHz component of the impulse couples to the output immediately while the 3.0-GHz component experiences the full filter delay.

Conversely, an upchirp signal with the proper frequency-delay characteristic applied to the downchirp ports of the filter is compressed into a pulse of width k/B_c and amplitude $(TB_c)^{1/2}$ above the input amplitude, where B_c is the chirp-filter bandwidth, T is the dispersive delay, and k is a constant near unity determined by the filter weighting function. This pulse is referred to as a compressed pulse, and the action of the downchirp filter on the upchirp signal is called matched filtering. As an example, k = 1.33 for Hamming weighting, giving a 0.44-nsec mainlobe pulsewidth for B_c = 3.0 GHz. The compressed pulse has sidelobes whose ideal amplitude depends on the weighting function, in addition to having a k/B_c mainlobe pulsewidth.

In direct analogy to a SAW grating or transducer array, the effective number of quarter-wavelength couplers N_{eff} active at a particular frequency f in a superconductive chirp filter with dispersive delay T and bandwidth B_c is

$$N_{eff} = f\sqrt{\frac{T}{B_c}}.$$

Thus, unlike the typical transversal filter, such as a charge-coupled device (CCD), in which the time delay between taps is constant and energy is tapped from a signal (for all relevant frequencies) across the full length of the device, the chirp filter effectively taps energy over only an N_{eff} grouping of couplers at a given frequency. This grating arrangement enables the chirp filter to produce a continuous downchirp or upchirp response, as shown in Figure 2(b).

Several techniques exist for designing superconductive chirp filters. Initial work used the coupling-of-modes theory [16]. More recent designs based on S- and T-matrix circuit analysis have been made possible by advances in computing power [17].

The material system of choice in early work on superconductive chirp filters was niobium on high-resistivity silicon. After initial demonstrations of the chirp-filter concept and a demonstration of a chirp-transform algorithm [18], further research yielded devices with error-sidelobe levels of –32 dB, and bandwidths as large as 6 GHz [19]. An error-sidelobe level is determined by the magnitude of nonidealities in a chirp-filter response, which can be calculated by using an analysis based on paired-echo theory [20]. In a compressed-pulse output, the error sidelobes rise above the designed sidelobe levels obtained for a particular filter weighting function. For example, with respect to the mainlobe, the ideal peak sidelobe level for Hamming weighting is –42.8 dB. An error-sidelobe level of –32 dB corresponds to a filter performance of 0.75-dB peak-to-peak amplitude accuracy and 5° peak-to-peak phase accuracy [21].

Reflectively tapped superconductive chirp filters were also designed and fabricated on the basis of a well-defined impedance discontinuity at the tap points [16]. However, this structure is susceptible to spurious reflections from defects and imperfections and has no input-to-output isolation, requiring a circulator for operation.

HTS Chirp Filters

The advent of high-T_c superconductors has provided an opportunity to move the concept of superconductive chirp filters into actual system applications. (For more information on the impact of HTS materials on microwave applications, see the sidebar entitled "Passive Microwave Applications for High-Temperature Superconductors," on the next page.) Initial work focused on materials and processing issues, with some design consideration peculiar to the high-dielectric constant substrates. Historically, one of the first HTS devices demonstrated was an 8-nsec, 3-GHz-bandwidth $YBa_2Cu_3O_{7-\delta}$ (YBCO) chirp filter [22]. This device was followed soon after by the demonstration of a 12-nsec, 3-GHz-bandwidth YBCO chirp filter [23, 24]. Finally, a matched pair of 12-nsec, 3-GHz-bandwidth YBCO chirp filters, one flat weighted and the other Hamming weighted, were used to generate a compressed pulse [25]. The matched filters exhibited –25-dB error sidelobe performance, consistent with 2.2-dB peak-to-peak amplitude accuracy and 14° peak-to-peak phase accuracy [21]. This performance is of comparable accuracy but at three times the bandwidth of the widest bandwidth SAW devices. The successful matched-filter demonstration paved the way for the High-Temperature Superconductivity Space Experiment (HTSSE) compressive cueing receiver described later.

Figure 3 shows the measured electrical characteristics of one of these 12-nsec Hamming-weighted filters, with a comparison between the designed and measured frequency-domain response. Chirp filters with the characteristics shown in Figure 3 were also used later in the HTSSE prototype receiver. As shown in Figure 3(a), 5 dB of insertion loss is designed into the filter, which limits the strength of the backward-wave couplers enough to avoid distorting the input signal as it propagates through the tapped-delay-line chirp filter. Dissipation loss in the filter is too small to measure.

These first chirp filters were fabricated in a typical stripline configuration with YBCO signal lines and two silver ground planes on $LaAlO_3$ substrates. The

PASSIVE MICROWAVE APPLICATIONS FOR HIGH–TEMPERATURE SUPERCONDUCTORS

THE 1986 DISCOVERY OF A NEW class of superconductors with substantially higher transition temperatures (T_c) offers the opportunity for greatly simplifying the cryocooling apparatus in most superconductor applications, making many more applications both economically and technically practical. The new superconductors, known as high-temperature, or high T_c, superconductors (HTS), are complex layered copper-oxide compounds that challenge material scientists to master difficult crystal growth methods.

The workhorse material has been $YBa_2Cu_3O_{7-\delta}$ (YBCO). It has a respectably high transition temperature of 93 K, and can more readily be grown in single phase than other HTS materials, resulting in high-quality thin films. A significant milestone in the development of thin films for microwave applications was the reliable and reproducible achievement of low surface resistance in YBCO at 77 K by many laboratories around the world. Figure A illustrates this achievement, circa 1992, with data compiled by H. Piel et al. [1]. Passive microwave devices benefit tremendously from the orders of magnitude lower surface resistance afforded by HTS thin films compared to normal metals.

Researchers have begun to implement a wide variety of planar thin-film HTS passive microwave applications. In contrast, active HTS microwave devices, such as mixers, that make use of the Josephson effect are still only in the early stages of development. In the main text, we introduce the advantages of planar HTS passive devices and describe a chirp filter based on long, tapped superconducting delay lines.

Another good example of planar HTS structures is a narrowband (high-Q) resonator-based filter that could previously be implemented only as a cavity filter. Figure B shows the size comparison between a compact planar HTS filter and an electrically similar bulky cavity filter. This size and weight difference becomes dramatic when numerous filters are used in a microwave system for channelizing a band of frequencies. Small size and weight are especially important for systems on mobile platforms such as aircraft and satellites. Figure C illustrates the effect of the low surface resistance of a superconductor on a narrowband microstrip filter [2]. The insertion loss of a filter can be estimated as

$$L_0 \approx \frac{434}{B(\%)} \sum_{i=1}^{n} \frac{g_i}{Q_{ui}}, \quad \text{(A)}$$

where L_0 is the center-frequency increase in attenuation (in dB) because of dissipation losses, B (%) is the fractional bandwidth in per-

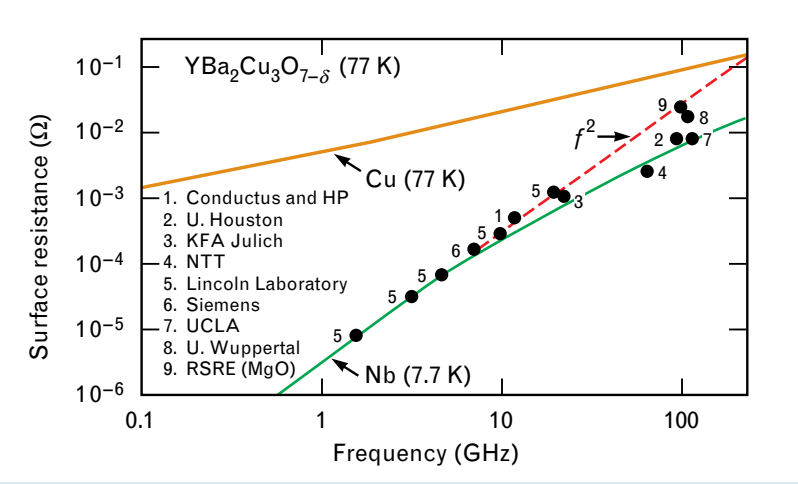

FIGURE A. Collection of measured surface resistance data at 77 K for thin films of YBCO from nine laboratories. The data are plotted as a function of frequency. The surface resistance of copper at 77 K and superconducting niobium at 7.7 K are shown for comparison.

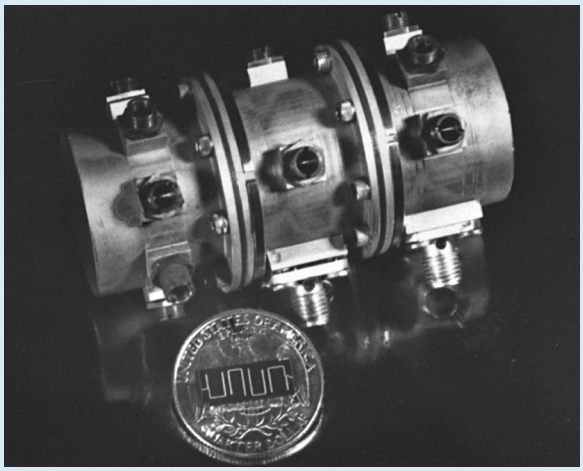

FIGURE B. Size comparison between a single (four-pole) superconducting microstrip filter and a single (six-pole) dual-mode dielectric-loaded cavity filter. The cavity filter is used in the input frequency multiplexer on a communications satellite. (Courtesy of COMSAT Laboratories.)

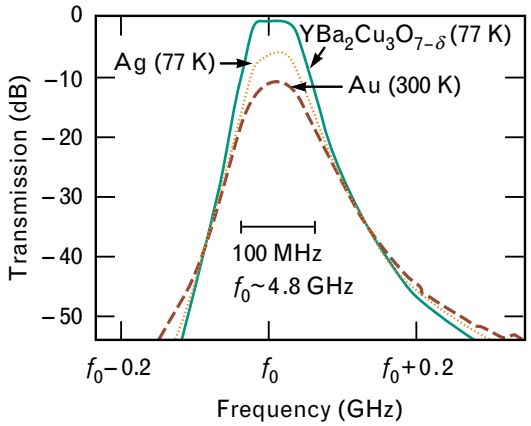

FIGURE C. Measured transmission response at 77 K of a four-pole-Chebyshev 1%-bandwidth YBCO microstrip filter. Measured responses of the same filter fabricated from silver (at 77 K) and gold (at 300 K) are shown for comparison. The superconducting filter exhibits a dramatic improvement in insertion loss and filter shape factor.

cent, g_i is the normalized series inductance and shunt capacitance of the low-pass filter prototype, and Q_{ui} is the unloaded Q of the ith resonator [3].

Equation A and the data of Figure C indicate that the transmission-line resonators comprising the filter in Figure B have unloaded Q values on the order of 150 for Au at room temperature, 250 for Ag at 77K, and 2000 for YBCO at 77 K. Soon we expect to demonstrate planar HTS patch-based resonators and filters with unloaded Q values greater than 150,000. This unloaded Q is higher than the unloaded Q values of most normal metal cavities. However, this performance in resonator-based devices can come at a price. The surface resistance of a superconductor is nonlinear at high fields (especially at temperatures approaching T_c), which generates intermodulation distortion and associated spurious signals. This intermodulation distortion must be characterized to ensure satisfactory performance of a device, particularly in transmitter applications [4].

Another example of an HTS passive microwave application is a millimeter-wave phased-array antenna feed. The effect of a superconducting feed network on phased-array antenna gain is shown for a 60-GHz array in Figure D, from Reference 5. The gain for the phased-array antenna is calculated as

$$\text{Gain (dBi)} = 20\log(D/\lambda_0) - 8.69\alpha D + 10\log(4\pi)$$

where dBi is gain in dB referred to isotropic radiation, D is the length of one side of the array, λ_0 is the wavelength in free space, and α is the attenuation coefficient (in nepers/m) of the microstrip feedline conductor. Figure E, from Reference 6, shows a prototype HTS feed structure. A second article in this issue describes the development of low-loss HTS-ferrite phase shifters that, together with an HTS feed network, will form a fully functional superconductive phased-array antenna. This antenna may offer a low-cost alternative to conventional active arrays that are based on monolithic microwave integrated circuits and place an amplifier at each element to overcome normal conductor distribution loss.

Other examples of passive microwave applications under development include probe coils for nuclear-magnetic-resonance

(NMR) spectroscopy systems, switched filter banks, electrically small antennas, superdirective antenna arrays, and tunable filters. HTS probe coils for NMR are offered as a commercial product, built by Conductus and available through Varian. Low-noise receiver front ends have been configured as hybrid systems that use cryocooled semiconductor devices with passive HTS filters. These low-noise front ends and sharp-skirted HTS filters may prove feasible even in the competitive wireless communications arena. Field trials in actual wireless base-station networks are under way with HTS-based receiver front ends built by Conductus, Superconducting Core Technologies, Superconductor Technologies Incorporated, and Illinois Superconductor.

References

1. H. Piel, H. Chaloupka, and G. Mueller, in *Advances in Superconductivity IV*, H. Hayakawa and N. Koshizuka, eds. (Springer-Verlag, Tokyo, 1992), pp. 925–930.
2. See Reference 23 in main text.
3. G. Matthaei, L. Young, and E.M.T. Jones, *Microwave Filters, Impedance-Matching Networks, and Coupling Structures* (Artech House, New York, 1980).
4. D.E. Oates, W.G. Lyons, and A.C. Anderson, "Superconducting Thin-Film $YBa_2Cu_3O_{7-x}$ Resonators and Filters," *Proc. 45th Annual Symp. on Frequency Control, Los Angeles, 29–31 May 1991*, pp. 460–466.
5. See Reference 27 in main text.
6. J.S. Herd, D. Hayes, J.P. Kenney, L.D. Poles, K.G. Herd, and W.G. Lyons, "Experimental Results on a Scanned Beam Microstrip Antenna Array with a Proximity YBCO Feed Network," *IEEE Trans. Appl. Supercond.*, vol. 3, no. 1, pp. 2840–2843 (1993).

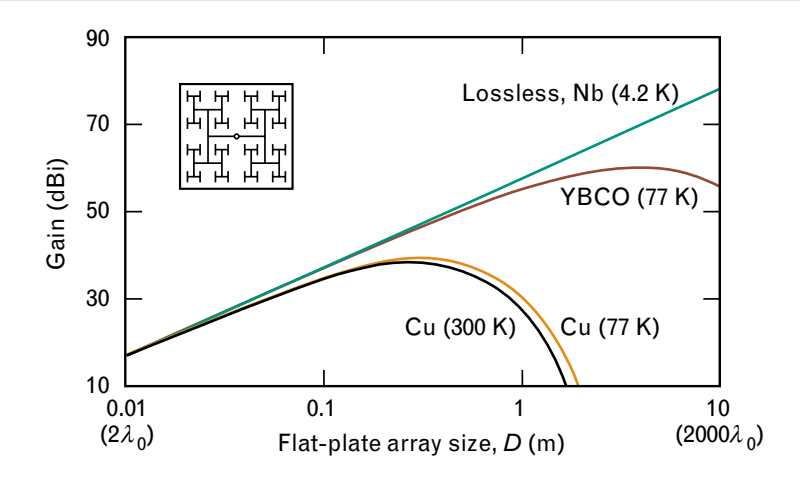

FIGURE D. Calculated effect of feed-network distribution loss on antenna gain for a 60-GHz phased-array antenna with various conductor materials in the feed structure. The calculation assumed the feed configuration shown in the inset with a $\lambda_0/2$ spacing between antenna elements (λ_0 = 0.5 cm at 60 GHz), and a 50-Ω microstrip transmission-line structure on a 10-mil-thick substrate with a dielectric constant of 10. The effect of the insertion loss of phase shifter elements was neglected.

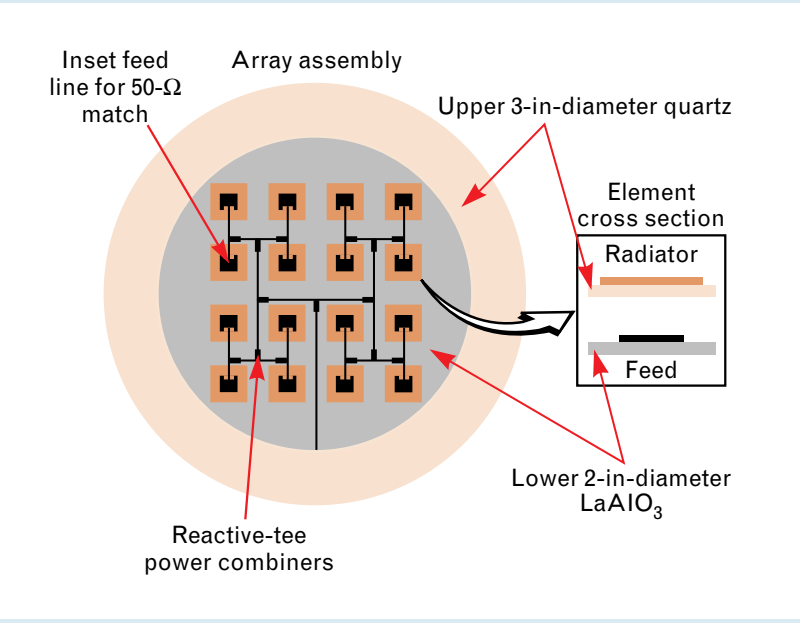

FIGURE E. Superconductive stacked-patch microstrip phased-array antenna geometry. The stacked structure produces a bandwidth of about 10% with a center frequency of 12 GHz. The upper quartz wafer was used as the dewar window of the vacuum chamber, and the lower $LaAlO_3$ wafer was thermally isolated from the quartz by a vacuum gap. Silver was used as the upper antenna-radiator element while the feed network and lower antenna element were patterned in YBCO.

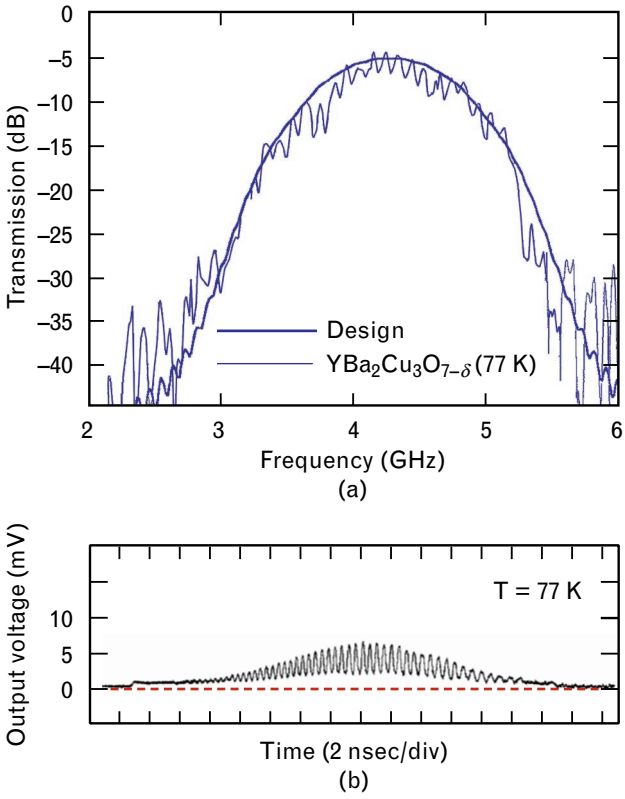

FIGURE 3. (a) Frequency-domain response of a Hamming-weighted YBCO chirp filter at 77 K. The chirp filter has a bandwidth of 3 GHz, a center frequency of 4.2 GHz, a (designed) insertion loss of 5 dB, and a dispersive delay of 12 nsec. (b) Downchirp time-domain response of a Hamming-weighted YBCO chirp filter at 77 K with the same parameters as in part *a*. The applied signal is a step function, and the response of each of the Hamming-weighted couplers can be discerned.

20-mil thickness of the brittle substrates limited the delay to 12 nsec to avoid excessive line-to-line coupling in uncoupled sections. $LaAlO_3$ has since become the substrate of choice for microwave applications because of its chemical, structural, and thermal-expansion match to YBCO, and its low microwave loss tangent. This low loss tangent is unusual for rare-earth perovskites.

An obvious discrepancy exists between the designed frequency response and the measured response shown in Figure 3. One of the challenges the $LaAlO_3$ substrate presents is the variation of the relative dielectric constant ε_r, due to the crystallographic twins in the rhombohedral material. Measurements of narrowband filters [1] and the variation in the time-domain reflectometry response of a microstrip spiral line are consistent with an ε_r variation in $LaAlO_3$ of 1 to 2% [1, 24]. Lower frequencies tend to average out the variation, while high frequencies and lumped-element circuits see a larger variation. Additional sources of degraded chirp-filter performance are YBCO film nonuniformity; wafer-thickness nonuniformity; impedance mismatch in the microwave transition from coaxial cable onto devices with a high-dielectric constant material (ε_r is approximately 23.5 in $LaAlO_3$); air gaps in the stripline caused by surface undulations (more severe because of twinning); and packaging effects, such as feedthrough. Figure 3(b) shows feedthrough in the time-domain response. Just past the first tick mark on the time axis, prior to the response of the first coupler, the signal jumps up slightly as a result of input-port to output-port feedthrough. Another large source of error is forward coupling, which is magnified by the length of the delay. This effect is absent in an ideal stripline device, but in an actual stripline device both air gaps and ε_r variations cause the even- and odd-mode velocities to differ slightly. This mode velocity difference results in nonideal backward-wave couplers with a nonzero coupling coefficient in the forward direction, thereby producing signals propagating in the wrong direction within the filter.

Throughout our work on HTS chirp filters, stripline has been the preferred structure for the transmission line, just as it was for niobium chirp filters. Microstrip has been an unacceptable structure for proximity-tapped chirp filters because of the unequal even- and odd-mode velocities, which result in tremendous forward coupling. Coplanar delay lines have the isolation and equal mode velocities required for backward-wave couplers, but require smaller dimensions than stripline to avoid moding problems, and are therefore more lossy than stripline. Some success has been achieved with coplanar waveguides for analog delay lines, but at the expense of inserting many air bridges to tie the two ground planes together [26]. Apparently the phase response of that coplanar structure is easily perturbed because of its similarity to a slow-wave filter, making a high-performance chirp filter difficult to achieve.

Despite the numerous burdens of cryogenic cooling, HTS chirp filters overcome many of the performance limitations of conventional filter technology. A 100-nsec proximity-tapped chirp filter in room-temperature copper stripline would exhibit 75 to 100 dB of dissipation loss in the range of 5 to 10 GHz [22, 27, 28], while an equivalent HTS chirp filter would produce negligible dissipation loss. In normal metal, dispersion caused by the frequency-dependent skin depth would also be a tremendous problem. The thick normal-metal layer required to achieve even the 75 to 100 dB of loss would add a further complication by introducing a large air gap into the stripline structure. Compared to SAW chirp filters, which often require ovens to generate a thermally stable environment, HTS filters are already in a temperature-controlled cryogenic environment. When operated at temperatures below approximately 60 K, YBCO HTS filters have little temperature dependence because the superconducting properties (order parameter and superconductor gap) change little below two-thirds of the transition temperature. SAW devices also produce at least 20 dB more insertion loss than HTS filters. Furthermore, because of the slow SAW propagation velocity, SAW devices are difficult to build accurately at those high frequencies where the structural dimensions become exceedingly small. Typical SAW wavelengths are on the order of 5 to 10 μm. Submicron lithography control must be applied to the transducer structures. The situation is different for HTS chirp filters because they are based on electromagnetic delay lines with wavelengths of many millimeters. This larger wavelength relaxes the dimensional control requirement somewhat, but lengths in the third dimension such as substrate thickness do become an issue.

Concept of Compressive Receiver

The concept of a compressive receiver based on chirp filters dates back almost forty years. Early work includes W.D. White's patent on the compressive receiver [29], as well as theoretical and experimental work by W.E. Morrow et al. [30]. The chirp-transform algorithm [8, 31–36], basis of the compressive receiver, can be understood mathematically if we start with a standard Fourier transform of a signal $h(t)$,

$$H(\omega) = \int_{-\infty}^{\infty} h(\tau) \exp(-i\omega\tau)\, d\tau, \tag{1}$$

and perform a linear mapping of frequency into time by substituting ω equal to μt, with μ the chirp slope (rate of linear frequency change with time). This linear mapping permits the following substitution in the complex exponent of Equation 1:

$$-i\omega\tau = i\mu\frac{(t-\tau)^2}{2} - i\mu\frac{t^2}{2} - i\mu\frac{\tau^2}{2}.$$

The expression for the Fourier transform becomes a chirp transform,

$$H(\mu t) = \exp(-i\mu\frac{t^2}{2}) \times \int_{-\infty}^{\infty}\left[h(\tau)\exp(-i\mu\frac{\tau^2}{2})\right]\exp\left[i\mu\frac{(t-\tau)^2}{2}\right]d\tau, \tag{2}$$

by using infinitely long chirp signals in the same way the Fourier transform uses infinitely long sinusoids. In Equation 2, the expression inside the first set of square brackets represents a multiplication of the signal $h(t)$ with a chirp signal. A chirp signal varies linearly in frequency over time and has a quadratic phase as a function of time. A convolution with a chirp of opposite slope is performed by the integration. Finally, another multiplication is done with a chirp signal of the same chirp slope as the first multiplication. Equation 2 is called a multiplication-convolution-multiplication (MCM) chirp transform and produces the complete Fourier transform of the input signal, where frequency, amplitude, and absolute phase are all mapped into time.

By taking the Fourier transform of Equation 2, and recalling that convolution in one domain becomes multiplication in the other and that chirps transform to chirps, we can demonstrate that a convolution-multiplication-convolution (CMC) configuration implements the same chirp transform. These continuous chirp transforms are not to be confused with a chirp-Z transform, which is a sampled version of this analog chirp transform and is imple-

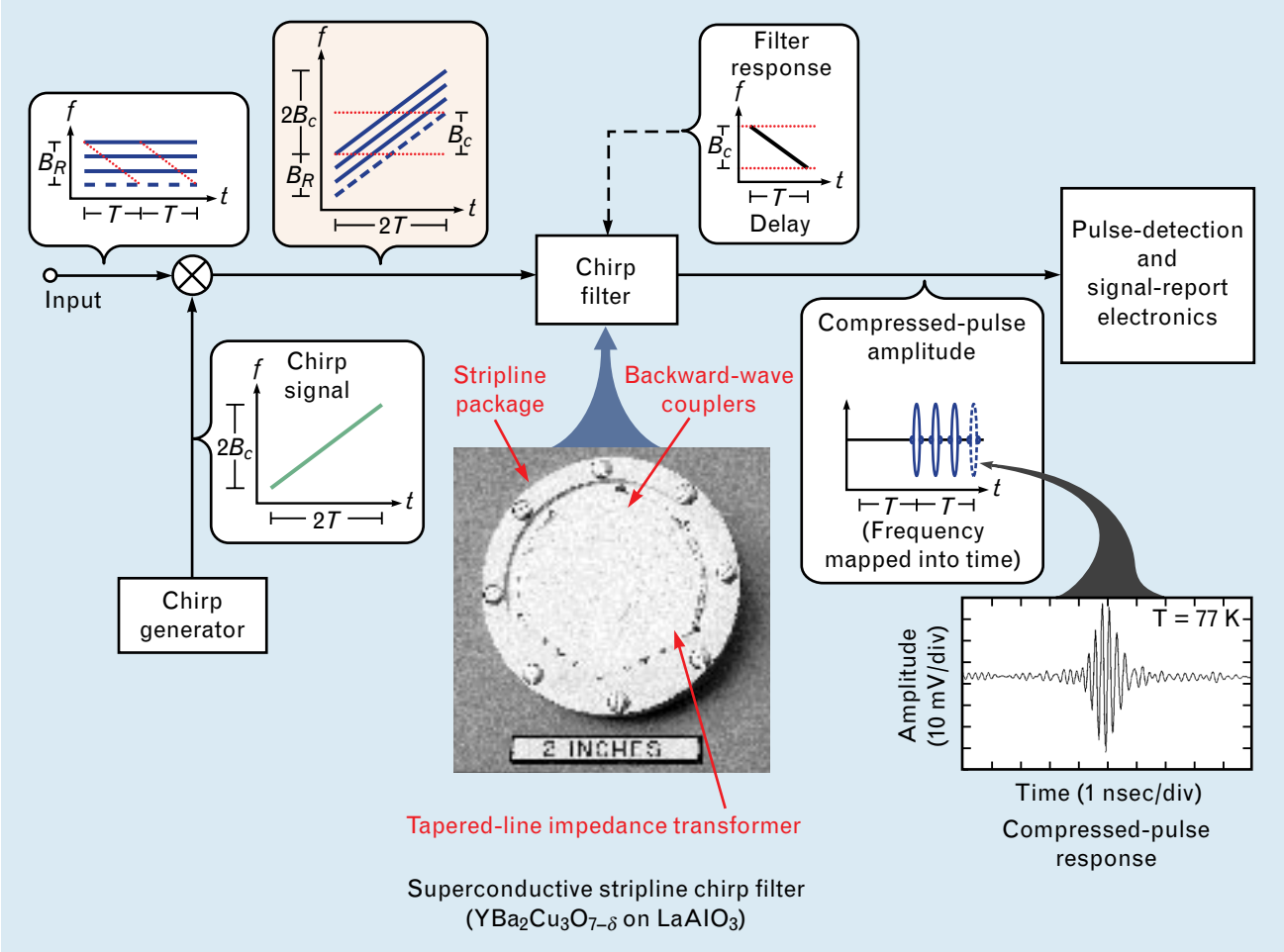

FIGURE 4. System diagram of a compressive receiver M(l)-C(s) chirp-transform algorithm with receiver bandwidth B_R, chirp-filter bandwidth B_c, and chirp-filter dispersive delay T. This architecture is well suited to extract the frequency and amplitude of input signals. The measured 77-K compressed-pulse response of a matched pair of YBCO chirp filters and a photograph of a 12-nsec YBCO chirp filter are shown as insets.

mented digitally or with CCDs [32]. In actual microwave implementations, multiplication with a chirp is performed with a chirped local oscillator and a mixer. Convolution with a chirp is achieved by passing the signal through a chirp filter. Actual implementations of the chirp-transform algorithm, however, cannot use the infinitely long chirp signals of the ideal mathematical expression indicated by Equation 2.

The finite length and finite bandwidth of actual chirp signals and real filters lead to two possible implementable full chirp transforms, the M(s)-C(l)-M(s) and the C(s)-M(l)-C(s), where l stands for long and s stands for short. Typically the long chirp is twice the length and bandwidth of the short chirp. Absolute phase information requires a full MCM or CMC chirp transform. If only the frequency, amplitude, and relative phase between two channels are required, the last M of the MCM or the first C of the CMC can be dropped. This requirement leaves two possible algorithms for a compressive receiver—M(l)-C(s) and M(s)-C(l). There are advantages to each [37]. The M(l)-C(s) system is used most often, but requires alternation between a pair of channels to achieve 100% time coverage. The M(s)-C(l) system requires only a single channel, but effectively halves the filter length for the convolution—C(l) must be twice the size of C(s) for the same frequency coverage—and a single-channel implementation has difficulty with out-of-band signals and filter triple-transit effects. An additional feature of the M(l)-C(s) system

Table 1. Frequency Resolution as a Function of Hamming-Weighted Chirp-Filter Dispersive Delay for an M(l)-C(s) Compressive Receiver

Dispersive Delay (nsec)	*Frequency Resolution (MHz)*	*Bins per GHz*
8	166	6.0
12	111	9.0
24	55.4	18.0
40	33.3	30.1
100	13.3	75.2
200	6.7	150.4

is the ability to readily increase frequency coverage by lengthening the multiplying chirp signal to overscan the bandwidth of the convolving chirp filter while maintaining the same chirp slope. This lengthening of the multiplying chirp signal extends the bandwidth coverage of the receiver at the expense of reduced time coverage. The M(l)-C(s) is often referred to as a microscan, or sliding-transform, receiver.

Figure 4 illustrates the operation of an M(l)-C(s) receiver. One of the four purple inputs (shown as frequency-versus-time curves) is dashed so that an input signal can be followed through the entire chirp-transform process. Input signals over the receiver bandwidth B_R are multiplied with a chirp signal of length $2T$ and bandwidth $2B_c$, with T the dispersive delay and B_c the bandwidth of the chirp filter. The multiplication (mixing) process produces a set of frequency-offset chirp signals (the beige balloon in Figure 4), in which each offset is determined by the input frequency. This set of chirp signals is convolved by the chirp filter, producing a compressed pulse at the output of the filter for each input signal. The exit time and amplitude of these compressed pulses are directly related to the frequency and amplitude of the input signal. The chirp filter must have the same chirp-slope magnitude but opposite sign relative to the chirp-signal generator. As indicated in Figure 4, mixing input signals over a bandwidth B_R with a swept local oscillator (SLO) of bandwidth $2B_c$ generates chirp signals that cover a frequency range $B_R + 2B_c$. Only B_c of that range lies within the bandwidth of the chirp filter, producing a compressed pulse. This relationship causes the input analysis window to be frequency dependent or slide in time, as shown in Figure 4 by the diagonal red-dotted lines superimposed over the input frequency-versus-time curves. Overscanning simply extends the SLO sweep to cover more bandwidth, and percent time coverage is inversely proportional to the overscan ratio. Referring to Figure 4, and assuming two alternating M(l)-C(s) channels for 100% time coverage of receiver bandwidth B_R with an SLO scanning over the scan bandwidth B_S, we define the following:

$$\text{overscan ratio} = \frac{(B_S - 2B_c) + B_c}{B_c} = \frac{B_S - B_c}{B_c},$$

$$\text{time coverage} = \frac{1}{\text{overscan ratio}}.$$

For example, to cover 10 GHz with a 3-GHz chirp filter requires an SLO scan of 13 GHz for a 3.3 overscan ratio and 30% time coverage.

Figure 4 highlights the HTS chirp filter as the enabling technology for a 3-GHz-bandwidth chirp transform. Conventional technology can be used to build the other chirp-transform components quite adequately, as is seen in later sections of this article.

Table 1 lists the frequency resolution $\Delta f = k/T$ of an M(l)-C(s) compressive receiver [6] that uses Ham-

Table 2. Pulsewidth (–3 dB) of Hamming-Weighted Compressed-Pulse Envelope and Pulse-Detection Logic Speed for 3.0-dB Amplitude Accuracy

Chirp-Filter Bandwidth	*Compressed-Pulse Width (nsec)*	*Pulse-Detection Logic Speed (gigasamples/sec)*
2.0	0.67	1.5
2.5	0.53	1.9
3.0	0.44	2.3
4.0	0.33	3.0
5.0	0.27	3.8
10.0	0.13	7.5
20.0	0.07	15.0

ming-weighted chirp filters, for which k = 1.33 [38] and where T is the dispersive delay of the filter. The range of delays shown is consistent with present HTS chirp-filter capabilities described later in this article. The compressed-pulse mainlobe width (–3-dB pulsewidth) is still k/B_c, as for the matched-filter example in the previous section on superconductive chirp filters. The frequency resolution Δf is determined by dividing the bandwidth B_c by the number of k/B_c pulsewidths (frequency bins) that fit into an analysis window of length T so that $\Delta f = B_c/[T/(k/B_c)] = k/T$, which is independent of B_c. Table 2 translates the –3-dB pulsewidth of the compressed-pulse envelope into a logic speed required to capture samples separated in time by this pulsewidth. This logic speed produces a 3.0-dB accuracy in determining compressed-pulse amplitudes.

Comparison of Receivers

A wide variety of receivers have been used in electronic warfare. The most common can be classified as superheterodyne, compressive, channelized filter, acousto-optic channelized, instantaneous frequency measurement (IFM), and crystal video receivers [8, 31]. Future receivers need to perform well in dense signal environments over many tens of GHz. The key requirements for future receivers are therefore excellent wideband simultaneous-signal performance and 100% time coverage of the bands of interest.

These considerations quickly eliminate crystal video, IFM, and superheterodyne receivers, and limit future advanced electronic-warfare receiver choices to compressive, channelized-filter, and acousto-optic channelized receivers. Crystal video and IFM receivers simply do not function well in the presence of more than a single emitter. Superheterodyne receivers have a poor probability of intercept (time coverage) because of their narrowband nature, despite their excellent dynamic range, sensitivity, and resolution [8]. A superheterodyne intermediate-frequency filter with a bandwidth B has a response time of $1/B$, and the fastest superheterodyne scan rate without degrading sensitivity is approximately $B/(1/B) = B^2$. As an example to point out the time-coverage limitations of superheterodyne receivers, if the intermediate-frequency filter bandwidth is 10 MHz, then the fastest scan rate is 100 MHz/μsec. If the input bandwidth is 10 GHz, then the superheterodyne receiver will take at least 100 μsec to scan across the entire band. There is a finite probability that the receiver will miss any pulses that are shorter than 100 μsec. In this example, at any one time the superheterodyne receiver is looking at only 0.1% (10 MHz out of 10 GHz) of the input bandwidth.

Among the remaining receiver candidates, channelized-filter receivers are considered in more detail in a later section as part of a direct comparison to an HTS compressive receiver. A major issue for channel-

ized-filter architectures is the large number of individual filters required. In contrast, acousto-optic channelized receivers [7] achieve channelization in a compact Bragg cell [39]. This arrangement is an efficient architecture, particularly for frequency activity indication. However, acousto-optic channelized receivers do have some potential weaknesses. The full parameterization of emitters is often slow because of the parallel nature of the receiver output and the need for quickly sampling these outputs. This parallel nature has forced the use of high-speed analog multiplexing circuits to serialize the channelizer output to a speed compatible with processing on a monolithic chip and at a frame rate fast enough to determine timing details (such as pulsewidth) of the intercepted emitters. The most mature acousto-optic technology (power-spectrum channelizer) does not allow relative phase information to be extracted, although acousto-optic heterodyne techniques are rapidly improving. Finally, the bulk-acoustic wave technology is limited to 2-GHz analysis bandwidths.

The significant challenge facing the development of HTS compressive receivers is the high-speed pulse-detection circuitry required because of the serial nature of the analog chirp-transform (compressed-pulse) output. As noted for acousto-optic receivers, data in a serial form have significant advantages if available circuits can achieve the required speed. Semiconductor technology is now producing circuits well matched to the multigigahertz bandwidths of HTS compressive receivers.

HTSSE II Compressive Cueing Receiver

Shortly after the discovery of superconductivity in the HTS material YBCO at temperatures near 90 K, engineers at the Naval Research Laboratory (NRL) became interested in the potential applications of using HTS electronic devices in high-performance remote sensing and communications systems. The low attenuation, wide bandwidth, low noise, and high speed associated with high-frequency superconductor applications are attractive attributes for these systems. In December 1988, NRL initiated the High-Temperature Superconductivity Space Experiment (HTSSE) program [40]. One goal of the HTSSE program was to accelerate the development of HTS into a viable electronic technology. Another goal was to focus HTS technology toward potential applications in space, which represents possibly the harshest environment in terms of reliability requirements, temperature extremes, and radiation levels. The HTSSE program consisted of two experimental payloads. The first experimental payload, known as HTSSE I, focused on simple HTS electronic devices. HTSSE I was completed in late 1992 and manifested on a satellite launch scheduled for 1993 that did not achieve orbit. HTSSE II addressed complex HTS devices and subsystems, and was shipped to Rockwell International in 1996 for integration onto the Advanced Research and Global Observation Satellite (ARGOS), scheduled for launch in 1997.

Lincoln Laboratory delivered both qualification and flight versions of an HTS wideband compressive cueing receiver—an example of a promising HTS subsystem—to NRL for HTSSE II [41, 42]. A cueing receiver is a spectrum activity indicator, producing frequency information on emitters that can be used to cue additional receiver assets onto active signals of interest [8]. This simplest form of a compressive receiver was chosen for the space experiment. The qualification and flight deliveries followed the production of a breadboard version of the receiver [43] and the delivery to NRL of a prototype [44]. All of the systems combine an HTS chirp-transform subsystem with high-speed semiconductor compressed-pulse processing circuits.

Figure 5 illustrates the operation of this receiver. An M(l)-C(s) chirp-transform algorithm is utilized with a 3.0-GHz-bandwidth YBCO chirp filter and a chirp generator consisting of a fast voltage-ramp generator driving a voltage-controlled oscillator (VCO) to produce a flat-weighted chirp signal. The compressed-pulse-detection portion of the system latches the value of a 2-GHz digital counter whenever a compressed pulse above a fixed threshold is detected coming out of the chirp-transform subsystem. This latching records the time a compressed pulse exits the chirp-transform subsystem and therefore records the frequency of the detected input signal via a lookup table. A 2-GHz oscillator serves as the clock generator that drives an 8-bit silicon emitter-coupled logic (ECL) ripple counter, which runs continuously. The

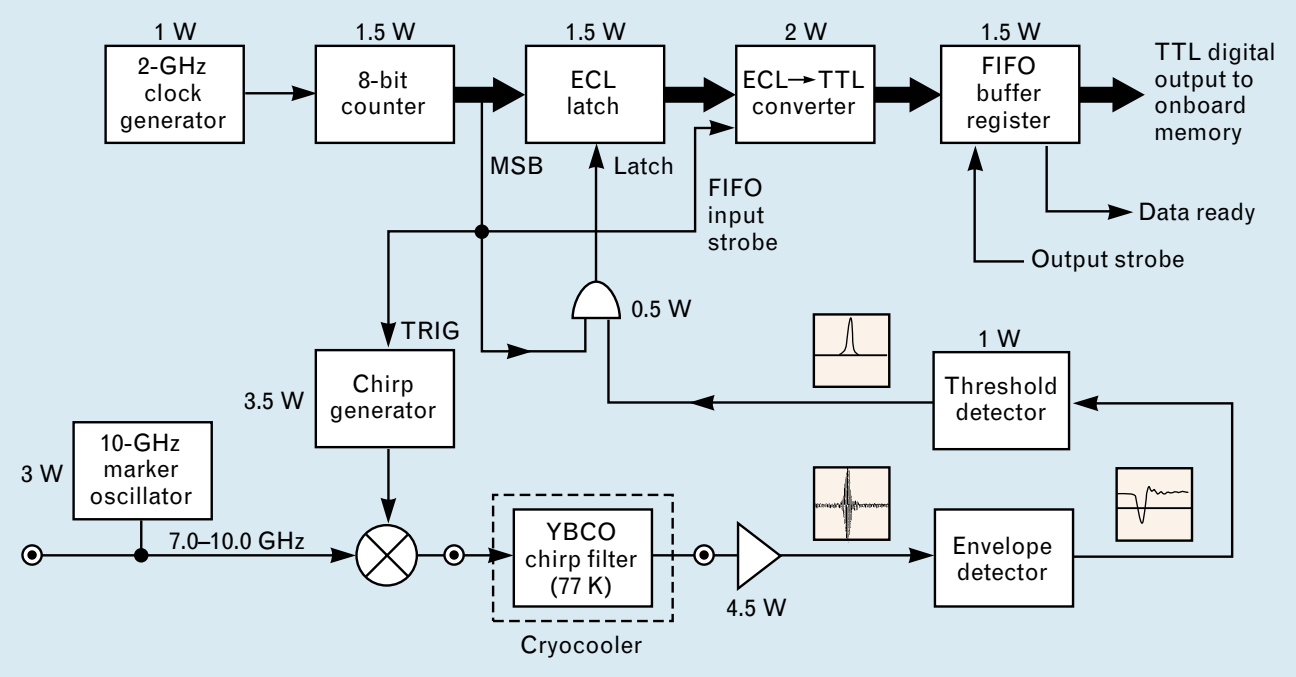

FIGURE 5. System block diagram of the High-Temperature Superconductivity Space Experiment (HTSSE) II compressive cueing receiver. Signal waveforms are shown as colored insets. The space-qualified version of the receiver covered a frequency range of 7.0 to 10.0 GHz, while the prototype covered a frequency range of 9.4 to 12.4 GHz. A 10-GHz oscillator was added to the input of the space-qualified receiver as an end-of-band marker. The power consumption indicated in the figure was measured on the space-qualified receiver.

most significant bit (MSB) is used as a reset trigger (TRIG) to the chirp generator, thereby setting the chirp-transform analysis window equal to $2^8 \times (0.5$ nsec), or 128 nsec. Valid data are accepted only when the MSB is high. The 2-GHz counter rate is required because a frequency bin corresponds to the –3-dB pulsewidth of a 3-GHz-bandwidth Hamming-weighted compressed pulse, approximately 0.5 nsec, as seen in Table 2.

A compressed pulse generated by a signal at the input to the receiver is passed through an envelope detector to remove the carrier frequency. This compressed-pulse envelope (negative portion of envelope) is then passed through a threshold detector (acting as an inverter) that strobes a silicon ECL logic gate to produce an appropriate logic level to latch the 8-bit counter value into an 8-bit ECL latch. The output of the counter is passed on to a first-in first-out (FIFO) buffer register following a voltage level conversion from ECL to transistor-transistor logic (TTL). The FIFO contents are then available to the satellite data bus and memory.

A 10-GHz oscillator was included on the qualification and flight versions of the receiver to produce an end-of-band marker for on-orbit receiver calibration. Figure 5 also indicates the power consumption of the various room-temperature components. The semiconductor ECL components are clearly costly to the power budget. The amplifier following the chirp filter is required to overcome the insertion loss of the mixer, cryogenic cables, and chirp filter, and then drive the envelope detector at a sufficient signal level to ensure linear performance from the detector. The compressed pulse, envelope-detected compressed pulse, and logic-compatible pulse waveforms are all shown as insets in Figure 5. Figure 6 shows a compressed pulse and compressed-pulse envelope typical of those produced by all versions (breadboard, prototype, qualification, and flight) of the compressive cueing receiver.

Projections of limited power available on board the satellite forced the Navy to restrict the cueing-receiver power budget to 20 W. Therefore, only the single ECL latch shown in Figure 5 could be included, lim-

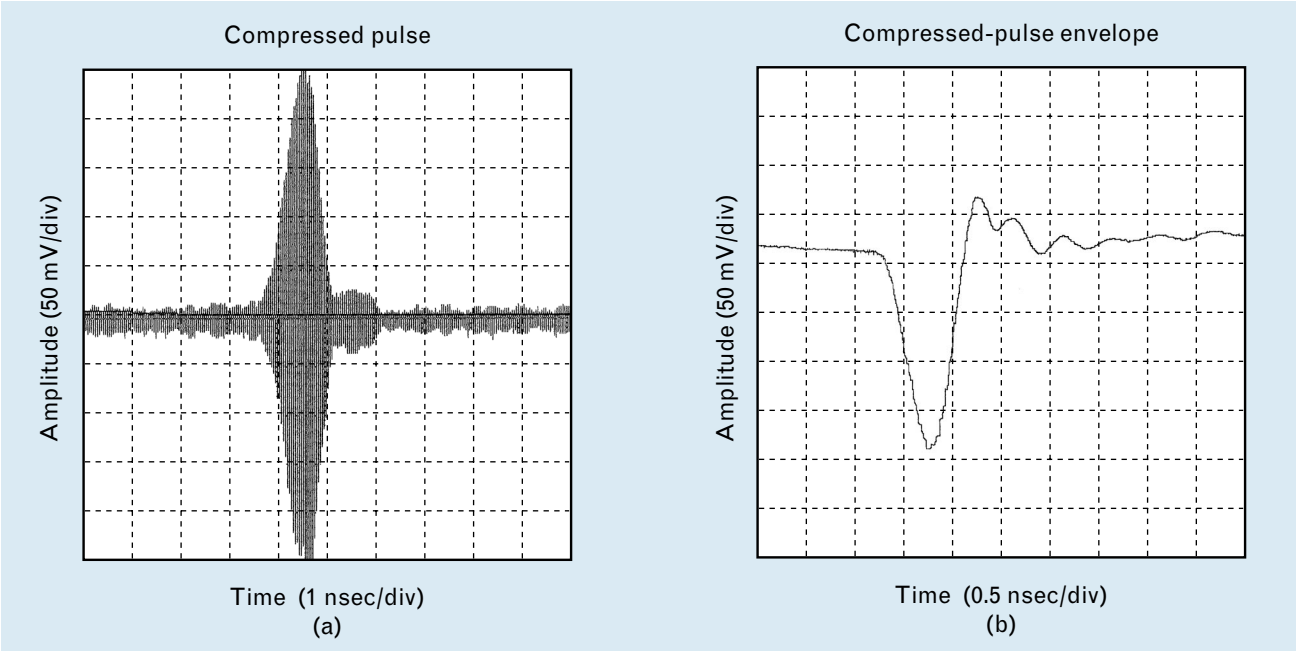

FIGURE 6. (a) Typical compressed-pulse output from the YBCO chirp filter in the HTSSE compressive cueing receiver. (b) Typical compressed-pulse envelope in the HTSSE compressive cueing receiver.

iting the receiver to determining the frequency of only one test signal within the 3-GHz instantaneous-analysis bandwidth. Multiple-signal capture has been previously demonstrated for this receiver configuration [43], but would have required a 4-W power increase per additional signal detection. As configured, the cueing receiver detects the 10-GHz oscillator signal (for end-of-band calibration) unless a test signal within the band of the receiver is being sent to the satellite from the ground. The test signal is then detected in the presence of the 10-GHz marker signal, demonstrating the capability of the receiver configuration to detect multiple simultaneous signals.

Figure 7 is a photograph of the prototype HTSSE compressive cueing receiver. The measured electrical responses of the YBCO chirp filter used in the prototype receiver are shown in Figure 3. Figure 8(a) shows the space-qualified 12-nsec cryogenic YBCO chirp filter. Figure 8(b) shows the space-qualified ambient-temperature electronics portions of the receiver. The addition of the 10-GHz oscillator and a shift in the chirp-filter center frequency from 4.2 to 6.7 GHz (to accommodate a 7.0-to-10.0-GHz input band) were the only significant differences between the prototype and flight versions.

Fabrication and Space Qualification of Hardware

The cryogenic YBCO chirp filter shown in Figure 8(a) has a stripline configuration, with an upper and a lower 2-in-diameter $LaAlO_3$ substrate squeezed together by an array of springs [25]. The upper substrate supports a single silver ground plane, while the lower substrate has the patterned YBCO tapped-delay-line chirp filter on one side and a silver ground plane on the other. The 165 BeCu springs hold the two substrates against an aluminum base plated with 125 μin of 24-K gold. The spring force generates enough static friction to prevent the substrates from moving under the specified mechanical stress. The base of the cryogenic filter package is clamped to the Navy's cryogenic bus by using spring-loaded bolts and an indium gasket. The cryogenic package is hermetically sealed to prevent degradation of the YBCO, which can occur when YBCO comes in contact with moisture and CO_2. The hermetic seal is implemented by sealing the package in a pressurized neon gas atmosphere with indium wire gaskets. The indium-wire-gasket technique is similar to a procedure extensively investigated for use with SAW devices on the Navy's Fleet Satellite Communications (FLTSAT) Extremely

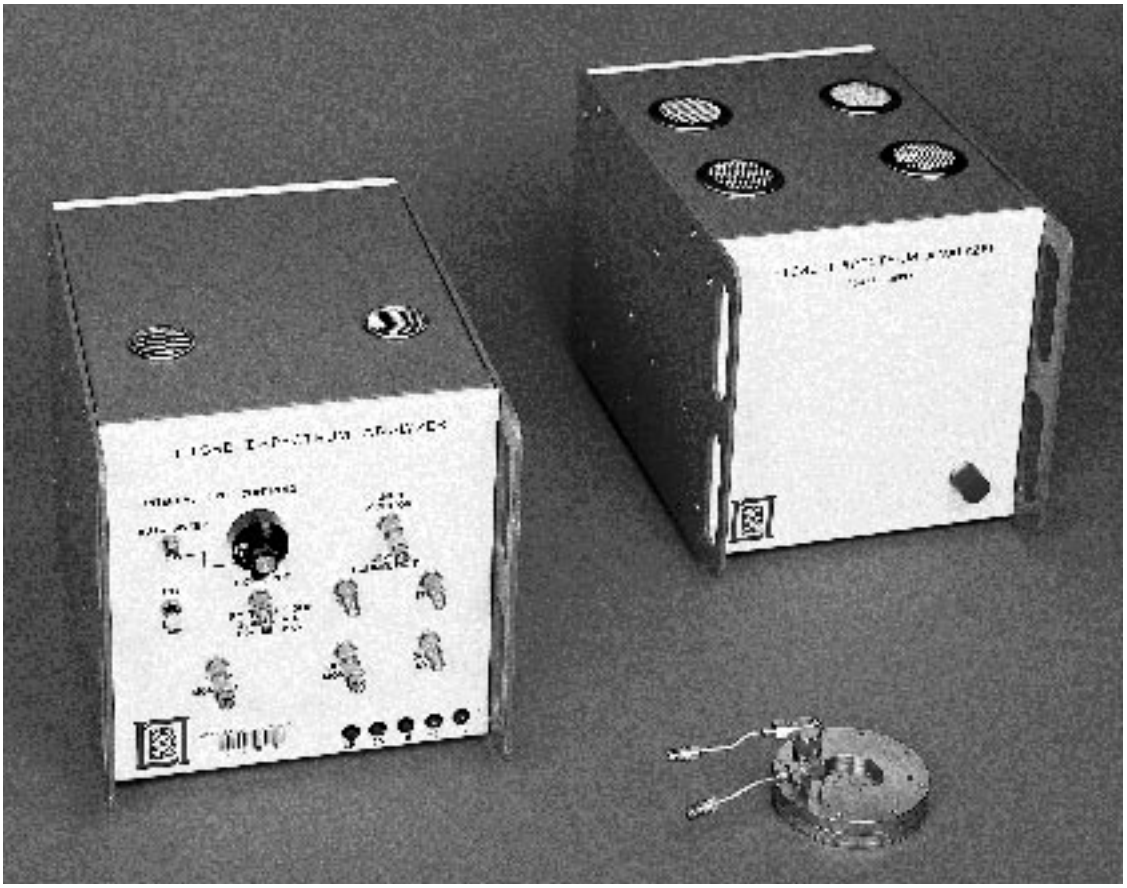

FIGURE 7. Prototype HTSSE compressive cueing receiver. The HTS chirp filter, room-temperature electronics box, and power supply box are shown.

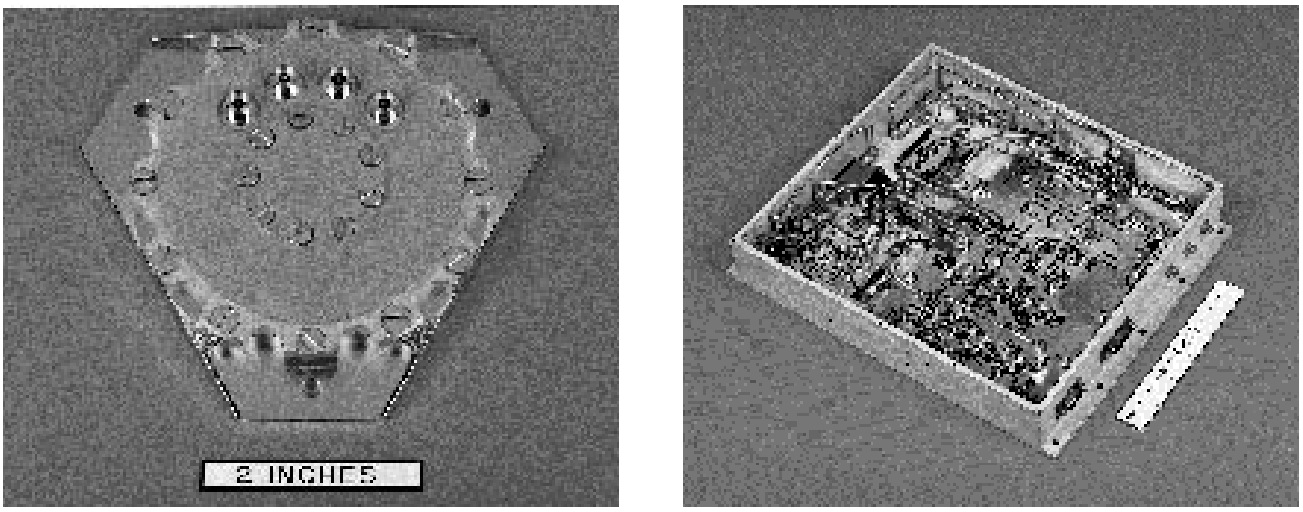

(a) (b)

FIGURE 8. (a) Space-qualified cryogenic package for the final HTSSE compressive cueing receiver. This hermetically sealed package contains the 12-nsec YBCO chirp filter in a stripline configuration. (b) Space-qualified package containing the ambient-temperature pulse-detection and frequency-report electronics, mixer, and chirp-generator portions of the final HTSSE compressive cueing receiver.

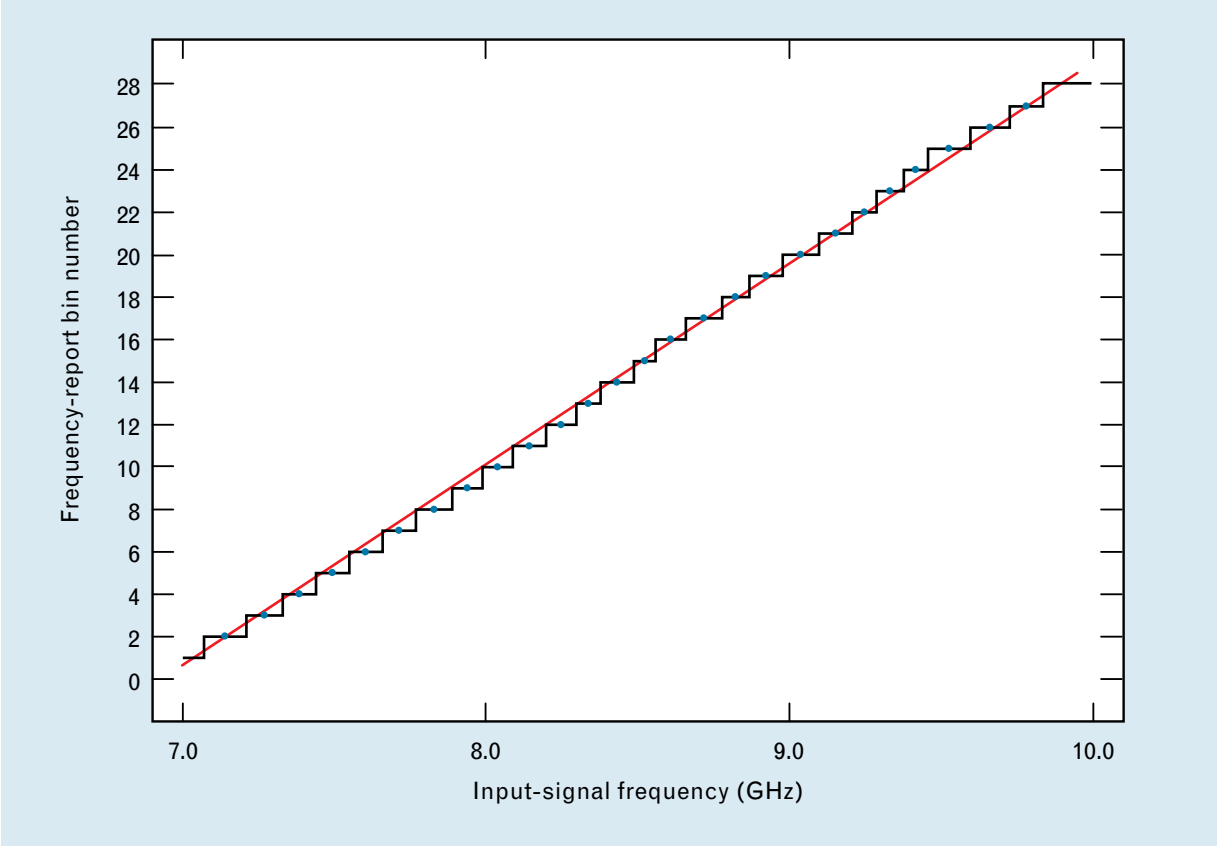

FIGURE 9. Frequency-report bin number versus input-signal frequency for the final flight version of the HTSSE compressive cueing receiver. The frequency midpoint of each frequency-report bin is indicated. The straight line shows the ideal location of each midpoint, which corresponds to uniform-width frequency bins. The average bin width (frequency resolution) is 110.0 MHz, equal to the ideal bin width for 12-nsec chirp filters. The maximum deviation from this ideal width is 30 MHz, and 40% of the bin widths are equal to 110 MHz.

High Frequency (EHF) Package, otherwise known as FEP [45], and the joint Lincoln/COMSAT/AT&T delivery of a narrowband YBCO filter for HTSSE I [46]. The cryogenic package was leak checked with a residual gas analyzer to establish a leak rate below 4×10^{-9} Torr-liter/sec. The package has a base footprint of seven square inches. Total package height is approximately 0.5 in, with an aluminum package base that is 0.13 in thick.

The fabrication of the YBCO chirp filter followed most of the standard procedures initiated prior to HTSSE I [1, 46]. A 4-μm layer of silver preceded by a 200-Å layer of titanium was used for both upper and lower ground planes. Patterning of the YBCO signal lines was accomplished with standard photoresist and a spray etch of 0.25% H_2PO_4, which successfully prevents the residual film formation typically seen with other wet-etching methods. Undercutting on the order of 1 μm is observed with this etch. Several techniques have been used for ohmic contact formation. The most successful technique has been a standard photoresist procedure with an in situ ion-beam etch followed by electron-beam evaporation of 1.5 μm of Ag. Following photoresist lift-off, the contacts are annealed in flowing O_2 for one hour followed by a slow ramp to room temperature. Final packaging for the space-qualified HTSSE II devices was performed by using ultrasonic wedge bonding of 0.5 × 3-mil Au ribbon directly on the annealed Ag contacts. These procedures yielded low contact resistances and good bond-pull strengths. The electrical responses of the space-qualified versions of the chirp filters were similar to those shown in Figure 3, with a shift in center frequency to 6.7 GHz. The HTSSE devices utilized

Table 3. Operating Characteristics of Final Space-Qualified HTSSE Compressive Cueing Receiver

Analysis bandwidth	3.0 GHz (7.0–10.0 GHz)
Frequency resolution	110 MHz
Frequency bins	28
Analysis time	128 nsec
Maximum cryogenic temperature	83 K
Cryogenic power consumption	5 mW (cables), plus radiative heat load
Total ambient power consumption	20 W (not including cryocooler power)

off-axis sputtered YBCO thin films [47] with typical best parameters of transition temperature T_c = 88 K, critical current density J_c (77 K) > 2 MA/cm^2, and surface resistance R_S (77 K, 10 GHz) = 500 $\mu\Omega$/sq. The 12-nsec length did not require values quite this low to achieve negligible dissipation loss. More recent work with longer delays has used films grown by a cylindrical magnetron, achieving these excellent parameters as standard performance [48].

Extensive work was performed to ensure that the ambient-temperature electronics box and the cryogenic YBCO chirp filter would survive an orbital rocket launch and the subsequent space environment. After a qualification version of both the ambient box and chirp filter were fabricated and tested, final flight versions were fabricated with any necessary modifications. Details on the space-qualification procedure are found in Reference 42.

Performance of the Final Space-Qualified HTSSE Cueing Receiver

Figure 9 shows a plot of frequency-report bin number versus input-signal frequency for the space-qualified HTSSE flight receiver. The number of frequency bins is determined by the width of the compressed pulses and the length of the chirp filter. The 3-GHz bandwidth and Hamming weighting of the chirp filter produce compressed pulses that are 0.44 nsec wide. The dispersive length of the chirp filter is 12 nsec. Therefore, the analysis window of the compressive receiver supports 28 frequency bins, providing the 110-MHz frequency resolution. Timing jitter on the order of 30 psec limited the definition of a bin width to approximately 10-MHz increments.

The chirp generator deviates from a linear frequency-versus-time slope significantly more than the chirp filter [43], and thereby sets an error-sidelobe level of 19 dB. These error sidelobes act just as spurious signals would in a compressive receiver, limiting the dynamic range of the system to 19 dB because of the single fixed threshold crossing used for compressed-pulse detection. A multiple-threshold receiver using the same technology could support a single-signal dynamic range of 60 dB and a two-signal dynamic range of at least 19 dB. The amplitude of the envelope-detected compressed pulse deviates by less than 3 dB across the 3-GHz analysis bandwidth.

However, this 3-dB pulse amplitude variation, which can be traced directly to nonlinearities in the SLO, has a significant effect on the width of each frequency-report bin. An increase in pulse amplitude causes the pulse to be detected sooner than the ideal, and a decrease delays the detection. Figure 9 indicates the frequency midpoint of each bin and the straight line illustrates the ideal location of each midpoint. While increases in pulse amplitude push the midpoint above the line and shorten the bin widths, decreases in pulse amplitude have the opposite effect. The movement of the midpoint with respect to the line (and the bin widths) closely tracks the measured compressed-pulse amplitude variation across the band, and can account for the maximum deviation of 30 MHz from the ideal bin width of 110 MHz.

Table 3 summarizes the operating characteristics

for the space-qualified compressive cueing receiver. The analysis bandwidth, frequency resolution, and number of frequency bins are readily evident from Figure 9. The 128-nsec analysis time is limited by the speed with which the chirp generator can reset itself and begin a new frequency sweep. Above 83 K the YBCO chirp filter is too close to the superconducting transition temperature to function properly. The ambient power consumption of 20 W is clearly dominated by the discrete high-speed semiconductor ECL logic operating at 2 GHz. A future version of this receiver would make use of rapidly emerging, commercially available, monolithic high-speed components that provide far greater digital processing capability with far less power consumption per gate.

Bonded/Thinned-Wafer HTS Chirp Filters

As indicated in Table 1, the frequency resolution of a compressive receiver is tied directly to the dispersive delay of the HTS chirp filters. The chirp filters are based on a stripline configuration that uses two symmetrically placed ground planes on opposite sides of a pair of wafers. If the line-to-line electromagnetic coupling is kept constant in a stripline configuration, then the packing density of the delay lines, and therefore the total chirp-filter length for a given substrate area, is inversely proportional to the thickness of the two wafers. Standard 20-mil-thick, 2-in-diameter $LaAlO_3$ wafers limit the delay, with appropriate line-to-line isolation, to approximately 12 nsec, as used in the HTSSE compressive cueing receiver. A bonded/thinned-wafer technique has been developed to increase the delay achieved on a 2-in-diameter $LaAlO_3$ wafer first to 24 nsec [49] and then to 40 nsec [50], a refinement of a technique used to demonstrate 44-nsec YBCO analog delay lines [28]. As the wafer thickness is reduced to 10 mil and less to allow more delay, a support wafer is required to prevent the thin wafer from breaking. Figure 10 illustrates the technique used to bond and thin a 2-in-diameter $LaAlO_3$ wafer, and shows a photograph of a 40-nsec YBCO chirp filter fabricated by using the technique.

The wafer-bonding process begins with a 20-mil-thick $LaAlO_3$ upper wafer with a sputtered layer of Ti/Au (300 Å of Ti followed by 2 μm of Au) on the bottom surface, a 20-mil-thick $LaAlO_3$ base wafer with a sputtered layer of Ti/Au on the top surface, and a 10-μm-thick gold foil. The two wafers and the gold foil must be kept very clean throughout the entire process. The wafers are forced together against the gold foil in a hot press inside an oxygen atmosphere.

The top wafer is lapped to a thickness of 190 μm, and then polished with chemical-mechanical polishing compound to a final thickness of 125 μm. The polished surface must allow for epitaxial growth of YBCO. After polishing, the bonded-wafer pair is placed in a standard gas-pocket heater developed by Lincoln Laboratory, and growth of YBCO is performed with our cylindrical magnetron on the top surface of the thin wafer [48]. Standard YBCO patterning techniques can be used following the YBCO growth. A layer of gold, electroplated onto the sides of the wafer, contacts the edges of the gold foil to complete the contact to the ground plane on the bottom surface of the thin wafer. The upper ground plane of the stripline configuration requires a second bonded-wafer pair.

We initially demonstrated 24-nsec YBCO chirp filters by bonding existing 10-mil-thick $LaAlO_3$ wafers to a 20-mil-thick $LaAlO_3$ carrier wafer and omitting the wafer-thinning step shown in Figure 10. For the initial demonstration of the 40-nsec YBCO chirp filters on 5-mil-thick $LaAlO_3$, we used the entire procedure indicated in Figure 10. The 24-nsec YBCO chirp filters with a modified HTSSE VCO-based SLO produced error sidelobes of –18 dB, limited by the frequency-slope linearity of the SLO [43]. The SLO generated an upchirp waveform, which was then compressed into a pulse by using the downchirp ports of the YBCO chirp filter. This setup is essentially an M(l)-C(s) receiver front end. However, the initial 40-nsec YBCO chirp filters produced error sidelobes of only –13 dB with a similar SLO [50]. The longer dispersive delay clearly made the device more susceptible to device imperfections such as forward coupling and poor microwave transitions. The 24-nsec filters consist of 96 backward-wave couplers, implemented in a 100-μm-wide 32-Ω stripline. The 40-nsec filters consist of 160 backward-wave couplers, implemented in a 100-μm-wide 24-Ω stripline.

We made improvements to the 40-nsec chirp filter by saw-cutting notches in the edge of the wafer and

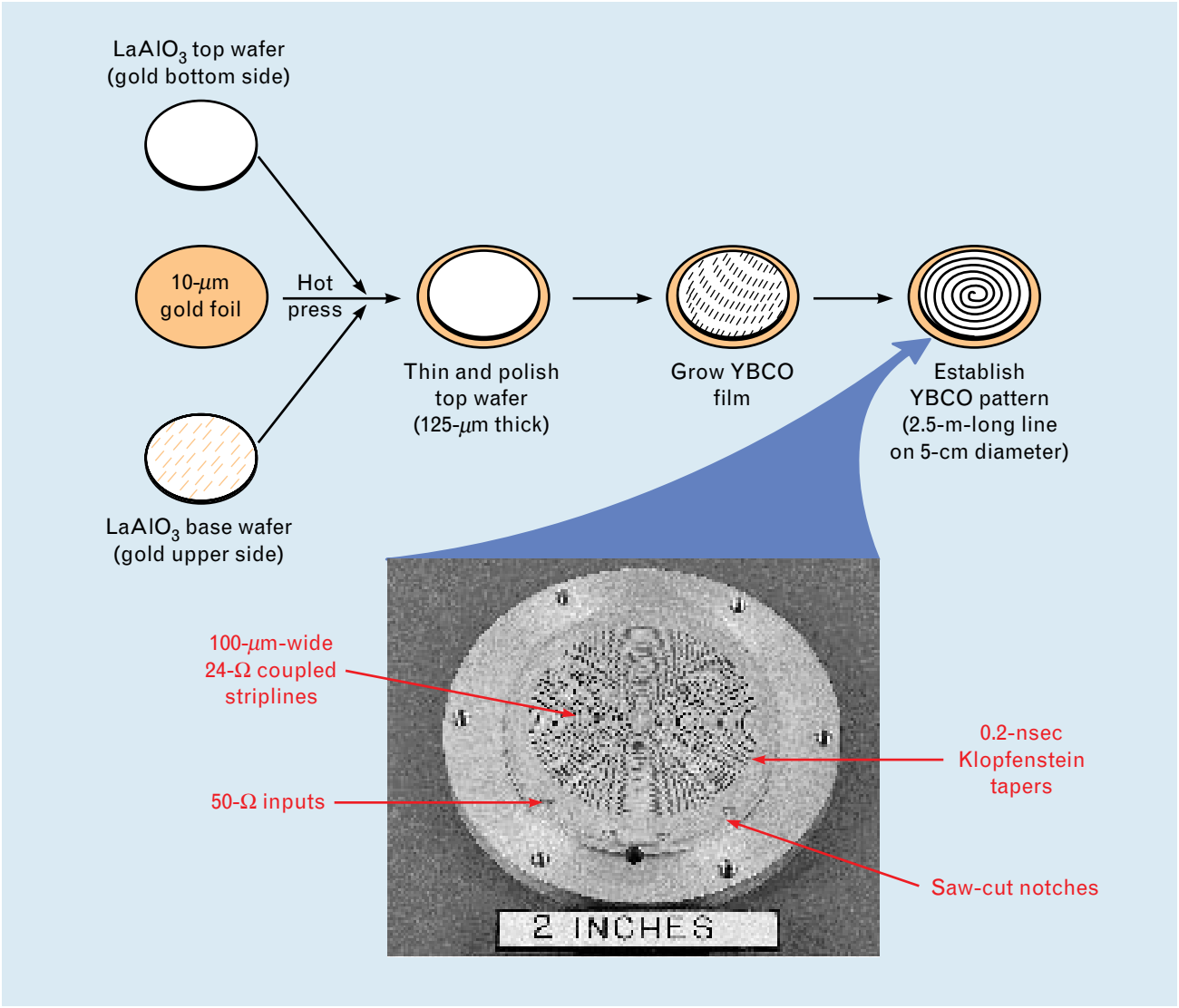

FIGURE 10. Illustration of bonded/thinned-wafer technique used to fabricate 40-nsec YBCO chirp filters on 125-μm-thick, 2-in-diameter $LaAlO_3$ substrates. The chirp filters are constructed in a stripline structure. A photograph of a Hamming-weighted 40-nsec filter is shown as an inset. The impedance transformers are based on a Klopfenstein taper [51].

gold-plating the inside of the notches. These gold-plated notches reduce reflections at the microwave transitions in and out of the filter. The YBCO film stops short of the edge of the $LaAlO_3$ wafer, requiring long bond wires and a nonstandard launcher configuration for the initial 24- and 40-nsec chirp filters. As shown in an inset to Figure 10, these saw-cut notches greatly reduce bond-wire length, allowing a more reasonable microwave transition to be made. The gold plating shortens the ground-plane contact path and therefore reduces inductance at the transition. We expect to improve the microwave transitions further.

The improved 40-nsec YBCO chirp filter produced –18-dB error sidelobes, once again the limit of the modified HTSSE SLO. Figure 11 shows this compressed-pulse performance for the combination of the SLO and the improved 40-nsec chirp filter. The measurement is made by the repetitive sampling of a digital oscilloscope to capture the compressed-pulse envelope.

The bonded/thinned-wafer technique used to produce 5-mil-thick substrates on 2-in-diameter $LaAlO_3$ wafers will scale directly to 3-in-diameter $LaAlO_3$ wafers, enabling dispersive delays of 90 nsec, or to 4-in-

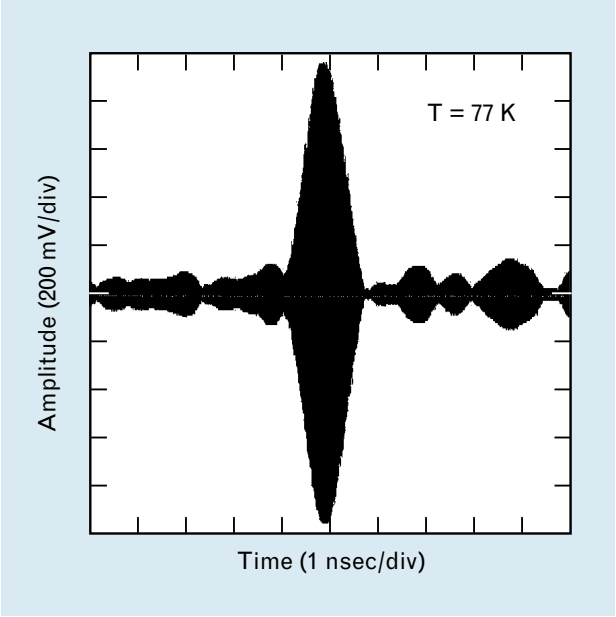

FIGURE 11. Compressed-pulse envelope measured at 77 K for the test setup combination of chirp generator and improved 40-nsec YBCO chirp filter. This setup produced SLO-limited error-sidelobe levels of –18 dB.

diameter $LaAlO_3$ wafers, enabling delays of 160 nsec. In both cases, thinner bonded substrates will produce longer delays. For these longer chirp filters, YBCO ground planes will be required to limit dissipation loss. This YBCO ground plane replaces the gold ground plane shown in Figure 10.

Demonstrations with Existing Compressive-Receiver Hardware

With Hughes Aircraft Company, we performed a demonstration with existing compressive-receiver hardware to produce the complete signal reports that are typically generated in a stand-alone electronic-warfare receiver [49]. In this demonstration, we replaced the 1-GHz, 200-nsec SAW chirp filters in the Hughes receiver with a 2-GHz, 24-nsec HTS YBCO chirp filter and VCO-based SLO. Although the analog and digital electronics in the Hughes receiver are matched to the narrower bandwidth of the SAW filters, the receiver was demonstrated to have full functionality with 2-GHz-bandwidth HTS chirp filters at the front end. This demonstration doubled the instantaneous bandwidth coverage of the receiver. An HTS chirp filter with at least 24 nsec of dispersive delay was required to fill a significant portion of the 200-nsec receiver analysis window to produce a meaningful demonstration.

The Hughes compressive receiver is a completely self-contained electronic-warfare receiver, capable of producing pulse descriptor words on multiple emitters. The descriptor words describe the emitter frequency, amplitude, pulsewidth, pulse-repetition interval, and time of arrival (TOA). The input frequency range for the demonstration was 9.8 to 11.8 GHz. A ramp generator and VCO combination functioned as a chirp generator to produce an up-chirp, using the M(l)-C(s) chirp-transform algorithm. Table 4 lists results of the Lincoln Laboratory–Hughes demonstration. The frequency-versus-time characteristic of the HTS chirp filter is significantly better than the characteristic of the VCO-based chirp generator, as described in the last section. The error-sidelobe levels set by the chirp generator act as spurious signals, limiting the single-tone dynamic range to 30 dB for a given signal detection threshold. A 50-dB dynamic range was obtained by adjusting the detection threshold. The receiver is limited to 200-nsec TOA resolution and only 50% probability of intercept for short pulses (100 to 400 nsec) because the receiver was designed to operate with 200-nsec-long SAW chirp filters and a 200-nsec analysis window. The frequency resolution of 83 MHz is limited because the receiver's 1-GHz log amplifiers elongate the 2-GHz-bandwidth compressed pulses generated by the HTS chirp filters. No more than three simultaneous signals can be detected because the detected compressed pulses must be at least 10 nsec apart, and the HTS chirp filter is only 24 nsec long.

Some preliminary demonstrations have also been done with linearized VCO-based SLO technology developed by AIL Systems [52, 53]. These demonstrations have resulted in reasonable performance from a combination of a linearized SLO and an initial 24-nsec YBCO chirp filter [54]. Future efforts should eliminate the SLO limitations described here.

Novel Wideband HTS Compressive Cryoreceiver

Figure 12 outlines a novel compressive cryoreceiver architecture. There are several key features to this new architecture, particularly the use of digital technology

Table 4. Summary of Lincoln Laboratory–Hughes Joint Compressive Receiver Demonstration [1,2]

Parameter	*Measured Performance*
RF input bandwidth	2.0 GHz
RF frequency resolution	2 GHz/24 cells = 83 MHz
Time of arrival and pulsewidth resolution	200 nsec
Dynamic range, single tone	30 dB [3]
Simultaneous signal detection	Up to 3
Short-pulse (100–400 nsec) probability of intercept	50%
Long-pulse (>400 nsec) probability of intercept	100%
Amplitude resolution	1 dB

[1] Taken from Reference 49.
[2] Performed with a 24-nsec, 2-GHz-bandwidth YBCO chirp filter.
[3] Greater than 50 dB with manual threshold adjustment.

to perform pulse detection and preprocessing. This architecture does not rule out the hybrid use of more traditional analog pulse detection [8], but allows receiver performance to be significantly improved. The cryoreceiver aspects of the architecture are generic to other types of microwave receivers.

Figure 12(a) illustrates the overall receiver and makes clear the potential for using additional cryoelectronic components to enhance performance. The overall receiver is a three-channel compressive receiver, using a monopulse antenna to determine angle of arrival by measuring monopulse-channel signal amplitudes only. (Relative phase extraction for interferometry could also be performed but would require double the pulse-processing electronics [21].) The configuration is an M(l)-C(s), and the signal reports are used to cue narrowband receiver assets for signal demodulation. These signal reports also represent a complete parameterization of frequency, amplitude, pulsewidth, time of arrival, and angle of arrival. The HTS delay line provides the local oscillator (LO) controller enough time to reconfigure. The expected length of HTS analog delay lines—up to 200 nsec—would stress the speed of the LO controller. Fast-tuned LO technology has been demonstrated with 100-nsec tuning times for smaller bandwidths [55], but has not yet been demonstrated for multigigahertz bandwidths.

Although the HTS chirp filters make the wideband compressive receiver possible, additional cryoelectronic components can significantly enhance receiver sensitivity and dynamic range. Initial demonstrations or investigations of many of these components have already been made. Cryocooled low-noise amplifiers [56, 57] and mixers [58, 59] can improve sensitivity by lowering the noise figure of the amplifier and reducing the conversion loss of the mixer. Adaptive notch filters [60] and tunable preselect filters [61, 62] can improve dynamic range by eliminating spurious signals or out-of-band noise. Any downconversion process is performed at cryogenic temperature [63] in conjunction with the SLO mixing with the input signals. An HTS delay line provides low loss and corresponding low noise figure to enhance the sensitivity of the superheterodyne receivers [26, 64].

The advanced semiconductor pulse-processing circuits shown in Figure 12(b) move the analog-to-digital (A/D) interface as close to the analog chirp-transform process as possible. An envelope detector strips the RF carrier from the compressed pulse, reducing the effective bandwidth of the pulse from that of the

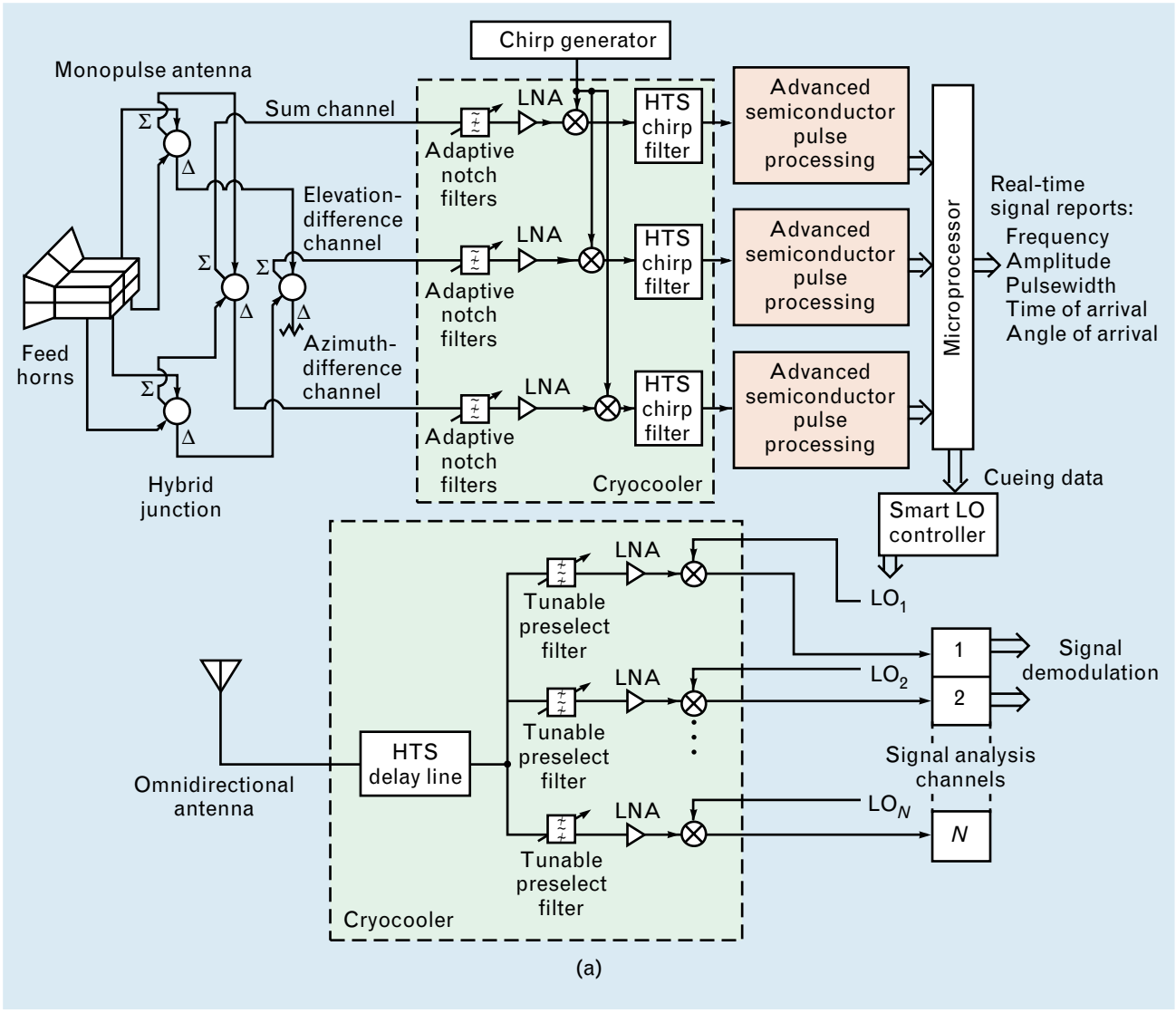

FIGURE 12. (a) Concept for compressive cryoreceiver, including cued narrowband cryoreceivers for signal demodulation. The compressive cryoreceiver core will produce real-time signal reports of frequency, amplitude, pulsewidth, time of arrival, and angle of arrival. These reports will then be used to cue the narrowband cryoreceivers. (b) Detailed schematic of proposed advanced semiconductor pulse-processing electronics of the compressive cryoreceiver.

carrier to that of the compressed-pulse envelope. This reduction greatly decreases the required analog bandwidth of the log amplifier and the sample rate of the A/D converter. The envelope detector and log amplifier precede a high-speed 6-bit 3-gigasample (GS)/sec GaAs heterojunction bipolar transistor (HBT) A/D converter [65] to provide a single-signal 60-dB dynamic range for a 4.0-GHz-bandwidth HTS compressive receiver. A demultiplexer circuit (DEMUX) reduces the clock rate requirement for the data-thinning application-specific integrated circuit (ASIC) [66]. The best choice for the ASIC is silicon-on-insulator (SOI) complementary metal oxide superconductor (CMOS), which is both high speed and low power [67–69]. Binary integration at the appropriate threshold level to enhance the sensitivity is performed over multiple analysis windows within each frequency bin of the receiver [70, 71]. The data-thinning process prevents overload of the digital signal processing (DSP) board. The thinned pulse-detection data are passed to a DSP board for frequency and amplitude accuracy enhancement through interpolation techniques that use knowledge of the pulse-envelope shape and a number of digital samples to determine the actual pulse centroid. These techniques should conservatively improve frequency accuracy, for example, by a factor of four. The techniques can also be used to identify the amount of partial window filling at the leading and trailing edges of a pulse to enhance pulsewidth or TOA accuracy. These pulsewidth and TOA enhancements contrast sharply with the difficulty that partial filling of the analysis window creates for analog pulse-detection techniques. Partial window filling substantially degrades pulsewidth and TOA accuracy to the length of an analysis window [8].

The use of binary integration to enhance sensitivity was previously demonstrated as part of a packet radio [70, 71]. In that communication application the phase of the carrier was known and the integrations were done coherently. In this case the integrations are noncoherent. A coherent integration process always yields a factor of N improvement in sensitivity, where N is the number of integrations, while a noncoherent process asymptotically approaches a factor of $4(N)^{1/2}$ improvement for a large number of integrations. However, for a small number of integrations the difference between coherent and noncoherent can be minimal [72]. This difference is somewhat a function of the false-alarm rate and probability of detection, i.e., the required minimum signal-to-noise ratio. For 100 integrations a coherent process yields a 20-dB improvement; a noncoherent process yields approximately 15 dB (not 10 dB, as an oversimplified $N^{1/2}$ calculation predicts).

For a further example, compare the use of binary integration, first with only a 40-nsec HTS chirp filter and then with both a 500-nsec SAW chirp filter and a 40-nsec HTS chirp filter. Recall that the sensitivity is independent of receiver bandwidth B_R, and that pulse compression is a coherent (analog) process equivalent to an integration. The 500-nsec SAW filter is 12.5 times longer than the HTS filter, but the HTS filter can have 12.5 noncoherent binary integrations performed in that time. The SAW filter alone has only 2 dB more sensitivity than the HTS filter with a noncoherent integration process because a small number of integrations is involved. The binary integration process can also be invoked for each 500-nsec frame of the SAW device. In the limit of a large number of integrations, the SAW device always performs 12.5 times fewer noncoherent integrations than the HTS device, giving it a maximum sensitivity advantage of 5 log (12.5) = 5.5 dB over the HTS device. But recall that the other cryoelectronic components in the HTS receiver enhance sensitivity, particularly at higher frequencies, in a way unavailable to a SAW system. This additional enhancement could equal or exceed the maximum 5.5-dB difference, while maintaining the short-pulse capability of the shorter HTS lines by avoiding partial filling of the analysis window for short pulses.

To establish a baseline for the amount of DSP required, we consider that only one set of DSP operations per pulse might be needed to enhance frequency accuracy. The processor then keeps track of that emitter on a coarser scale. If we assume a generic 1-Mpulse/sec signal environment and assume a conservative 25 operations to determine the pulse centroid, a processing rate of only 25 mega floating-point operations per second (MFlops) is required. This rate is 10^4 times less than the operations required to implement an all-digital receiver. At this level, the

DSP circuitry requires only a small fraction of the receiver size, weight, and power. Enhancement of TOA through DSP operations to identify the amount of partial analysis-window filling at the leading and trailing pulse edges would require an additional 50 operations per pulse, producing a total requirement of 75 MFlops.

Some size, weight, and power estimates can be made by accounting for the cryocooler and its control electronics. A typical cryocooler/controller combination (Stirling cycle) will require 25 to 50 W, 0.5 to 2.0 kg, and 0.1 to 0.2 ft^3 for 0.5 to 1.5 W of cooling power near 70 K. The receiver system described, making use of new semiconductor monolithic components, translates into a small number of ASIC chips per channel, possibly on a single board. This receiver solution can readily be estimated to consume well under 200 W for a three-channel compressive receiver. The receiver architecture is also better suited to handle wider bandwidths than a receiver approach based on multiple analog pulse-detection and processing boards. Timing uncertainties between boards would preclude their use for bandwidths of 20 GHz, in which timing accuracies of less than 10 to 20 psec would be the norm.

The proposed HTS compressive cryoreceiver architecture is capable of unprecedented multigigahertz bandwidth coverage per channel, translating into a receiver of small size, weight, and power. Compared to SAW receivers, the HTS receiver could have the same or better sensitivity, similar frequency accuracy and resolution, the same or better amplitude accuracy, greatly improved TOA and pulsewidth accuracy, improved dynamic range, and greatly improved short-pulse capability.

Comparison to Conventional Technology

HTS-Compressive versus All-Digital Receiver

The signal processing power of an analog Fourier-transform process becomes evident with a comparison to the equivalent digital fast Fourier transform (FFT) process in floating-point operations per second (Flops) to achieve the same frequency accuracy and resolution. Recall that an N-point FFT has a frequency resolution of $1/(NT)$ Hz, where T is the sampling interval [73]. The maximum frequency that can be sampled and satisfy the Nyquist criterion is $f_{max} = 1/(2T)$ Hz. As long as the signal of interest can be brought down to baseband, f_{max} is equal to the receiver analysis bandwidth B_R. Performing an FFT in real time requires that the FFT be completed during the signal, which is a time equal to NT. Assuming N is a power of two, $(N/2)\log_2 N$ butterfly operations are required for an N-point FFT [74]. The modern SHARC DSP chip (Analog Devices ADSP-2106X) performs an N-point complex FFT in $2N\log_2 N$ clock cycles with 3 Flops/cycle (120 MFlops at a 40-MHz clock rate) [74], resulting in the following DSP rate to perform an N-point complex FFT:

$$\text{DSP rate (Flops)} = \frac{19.92}{NT} N \log_{10} N$$
$$= 2 f_{max} (19.92) \log_{10} N .$$

Table 5 lists examples of the digital equivalents in Flops for analog chirp-transform algorithms relevant to HTS and SAW compressive receivers.

We recognize that round-off "noise" will require extra bits to be carried internally to support the desired dynamic range in the DSP FFT [75]. For an N-point FFT based on internally scaled fixed-point arithmetic, the power ratio of round-off noise to ideal output is $4N(2^{-2b})$, where b is the number of bits carried in the computation. Fixed-point DSP chips usually clock slightly faster than their floating-point counterparts. A dynamic range of 2^{b_0} requires $b = b_0 + (1/2)\log_2 4N$, where $(1/2)\log_2 4N$ is the number of additional bits needed internally. For example, a 60-dB dynamic range in a 1024-point FFT internally requires 16 bits to provide an output of 10 bits.

The success of very-large-scale integration (VLSI)/ultra-large-scale integration (ULSI) CMOS and BiCMOS circuits has led to dedicated fixed-point and floating-point DSP chips. As an example, the MeshSP-1 synchronous processor [74] is an 8×8 array of sixty-four SHARC DSP chips and is capable of 7.7 GFlops throughput requiring approximately 100 W for two 7.25 × 13-in circuit boards. This is approximately the equivalent of a 50-MHz-bandwidth 40-μsec-long analog chirp-transform algorithm in a

Table 5. Digital Signal Processing Equivalent (Flops) for Various Compressive Receivers

Bandwidth (GHz)	*N*	*Duration NT (nsec)*	*Frequency Resolution (MHz)*	*Equivalent DSP Rate (GFlops)*
HTS Compressive				
10.0	2048	102.4	9.8	1320
3.0	512	85.4	12	324
3.0	256	42.7	23	288
3.0	128	21.3	47	252
SAW Compressive				
1.0	256	128	7.8	96
0.30	8192	13,660	0.073	47
0.30	128	213	4.7	25
0.050	4096	40,960	0.024	7

SAW compressive receiver. Scaling the MeshSP-1 processor directly by a factor of 40 to 300 GFlops would require a minimum 4 kW of power and over 2500 DSP chips. This digital solution is clearly not a small size, weight, and power solution, and requires more than ten times the power estimate for the HTS compressive receiver.

HTS-Compressive versus Channelized-Filter Receivers

A comparison to channelized-filter architectures can also be made by determining the minimum number of filters required in a filter bank to achieve the same frequency accuracy as the novel HTS compressive-receiver architecture described in the last section. Table 6 lists examples of this comparison for 3-GHz and 10-GHz-bandwidth receivers. If the comparison focuses on the core function of the receiver and assumes that the signal-report electronics is either separate or consumes a negligible fraction of the receiver, then a compressive receiver consisting of a single HTS chirp filter in a cryostat and several ASIC chips for pulse detection (and signal report) could reasonably consume ten times less size and weight than 3000 RF filters. Interpolation techniques would reduce the required number of filters at the expense of added complexity.

The channelized-filter approach must also contend with the transient (or rabbit ear) phenomenon in which the $\sin(x)/x$ sidelobe components of a received RF pulse spread out into adjacent filter channels, compromising receiver performance [8]. This transient phenomenon is a particularly difficult problem for short RF pulses. The compressive receiver, in contrast, divides each received pulse into smaller analysis windows that are weighted (Hamming weighting is a good example) to produce small, well-behaved sidelobes. Introducing such a weighting scheme into a channelized-filter approach adds greatly to the receiver complexity. Gaussian-weighting each of the channelized filters helps somewhat, but the channelized-filter bank must contend with the frequency sidelobes produced by the input signal. An alternative measure is to use two filters in cascade for each channel, the first a narrower bandwidth with few poles and the second a wider bandwidth with many poles. This modification has the drawback of adding to the size and weight of channelized-filter receivers. The transient phenomenon also makes the use of interpolation more difficult.

The transient phenomenon often forces the use of wider bandwidth channels than desired in a channelized-filter architecture, thereby degrading sensitivity.

Table 6. Projections for Frequency Accuracy of Wideband Compressive Receiver with 100-nsec HTS Chirp Filter[1]

	Frequency Accuracy (MHz)	*Equivalent Number of Channelizing Filters[2]*
HTS Compressive Receiver (3-GHz BW)		
Without interpolation	13.3	225
With conservative interpolation	3.3	900
HTS Compressive Receiver (10-GHz BW)		
Without interpolation	13.3	750
With conservative interpolation	3.3	3000

[1] Compressive receiver can be configured by using only one HTS chirp filter.
[2] Assumes channelizing-filter architecture does not use interpolation.

A compressive receiver can be configured with 5 to 10 dB better sensitivity than a channelized-filter receiver [6]. For comparison purposes, the sensitivity of a compressive receiver can be calculated by using the noise over the entire bandwidth B_R of the receiver along with the TB_c signal processing gain or the noise over the frequency resolution bandwidth $\Delta f = k/T$ without the signal processing gain. These two methods are equivalent and point to the excellent sensitivities obtainable with compressive receivers. However, the channelized-filter approach does currently offer an advantage in two-signal spurious-free dynamic range over an HTS wideband compressive receiver. This benefit could, depending upon the application, outweigh any sensitivity advantage.

Future Developments

There are no physical limitations to prevent near-term advances in both HTS chirp-filter technology and the advanced semiconductor circuits described previously. The HTS chirp filter is based on electromagnetic delay lines. The low measured losses in HTS thin films combined with careful RF design should allow the bandwidths of HTS chirp filters to reach 20 GHz. The accuracy of HTS chirp filters will also continue to improve. The most notable improvement will come from the use of new substrate materials to replace $LaAlO_3$, which suffers from a random variation in its dielectric constant because of crystallographic twins. Cryocooler efficiency, reliability, size, and weight will continue to improve, driven by infrared and HTS technologies. Transition temperatures of HTS materials may improve somewhat as well. Cryocooled semiconductor digital components and even HTS digital components [76] are much longer-term possibilities.

We can project the near-term future of the advanced semiconductor circuits described in this article. Moore's Law and variations thereof tell us that circuit densities and speeds in VLSI/ULSI CMOS have doubled roughly every 18 to 24 months, a trend that will continue until a physical and economic limit is reached [77]. A 6-bit 3.0-GS/sec A/D will eventually be replaced by a 6-bit 10-GS/sec A/D, and so on. The capability of DSP chips will improve as measured in both clock speed and operations per second. We project that the capabilities of SAW compressive receivers (≤100 GFlops) will be surpassed in the next ten years by all-digital receivers consuming less than 100 W. In contrast, the equivalent digital signal processing capability of HTS compressive receivers will approach 3 TFlops over the same time frame in a much smaller size, weight, and power package than would be possible in an all-digital receiver.

Conclusions

HTS chirp filters have matured to represent an enabling technology for compressive receivers with

bandwidths greater than 1 GHz. HTS compressive receivers have the widest instantaneous analysis bandwidth per channel for any receiver technology, significantly above the 2-GHz limit of acousto-optic channelizer technology. This wide bandwidth translates into a receiver with small size, weight, and power requirements.

Dispersive delay in HTS chirp filters has been increased to 40 nsec by using a bonded/thinned-wafer technique, giving time-bandwidth products in excess of 100. Chirp filters with multigigahertz bandwidths have been demonstrated in YBCO stripline structures with 24-nsec dispersive delay on 10-mil-thick, 2-in-diameter bonded-wafer $LaAlO_3$, and with 40-nsec dispersive delay on 5-mil-thick, 2-in-diameter bonded/thinned-wafer $LaAlO_3$. Both 24- and 40-nsec filters have produced better than –18-dB error sidelobes. Chirp filters had previously been demonstrated with 8 and 12 nsec of dispersive delay in YBCO on self-supporting 20-mil-thick, 2-in-diameter $LaAlO_3$.

Several compressive receivers have been reported here that function at bandwidths unavailable with conventional chirp-filter technology. A space-qualified HTS compressive cueing receiver was designed and built for flight in the Navy's HTSSE space experiment on the Air Force ARGOS scientific satellite. The 3.0-GHz instantaneous analysis bandwidth demonstrated in the prototype and space-qualified HTSSE compressive cueing receivers was unprecedented. This HTSSE cueing receiver provided a frequency resolution of 110 MHz with a 19-dB dynamic range over a 7.0-to-10.0-GHz input band. In addition, an existing Hughes compressive receiver, operated as an HTS compressive receiver, demonstrated a frequency resolution of 83 MHz with a 50-dB dynamic range across a 2.0-GHz band from 9.8 to 11.8 GHz. This modified receiver detected up to three simultaneous emitters with a 1-dB amplitude resolution and 100% probability of intercept for pulses greater than 400 nsec.

Here we have proposed a novel compressive cryoreceiver architecture, combining HTS, cryoelectronic, and advanced high-speed semiconductor technologies. This compressive receiver architecture will readily rival the sensitivity of a narrowband receiver while providing instantaneous frequency coverage of up to a 4-GHz band with a 3.0-GS/sec A/D immediately following the analog chirp-transform subsystem. The high-speed serial nature of the compressive receiver output is well matched to emerging semiconductor components. Future technology developments are poised to extend this bandwidth capability. The opportunity for insertion of additional HTS and cryoelectronic components to enhance receiver sensitivity and dynamic range makes the wideband compressive receiver an attractive application of analog HTS microwave filters. Relatively short 40-nsec HTS chirp filters produce good short-pulse analysis capability, but not at the expense of other receiver parameters. In fact, the novel features of the proposed receiver will improve many parameters over SAW compressive receivers, particularly with respect to the wideband, real-time simultaneous-signal analysis capability, and size, weight, and power requirements.

Applications exist for this receiver in electronic warfare and remote sensing. Detailed comparisons of the HTS wideband compressive receiver (including cryocooler) to an all-digital receiver and to channelized-filter receiver architectures have identified the compressive receiver as superior to the others by better than one order of magnitude in size, weight, and power. Several important advantages of HTS compressive receivers over acousto-optic channelizers have also been noted, especially the wider bandwidth coverage per receiver channel.

Acknowledgments

This work was supported by the Naval Research Laboratory (NRL) under the High-Temperature Superconductivity Space Experiment (HTSSE) program, by the Department of Defense, and by the Defense Advanced Research Projects Agency (DARPA), in part under the auspices of the Consortium for Superconducting Electronics.

The authors acknowledge the collaboration of Robert Guadagnolo and David Barry of Hughes Aircraft Company in demonstrating the functionality of HTS chirp filters with a Hughes conventional electronic-warfare compressive receiver; and Joseph Levy and Peter Burke of AIL in demonstrating the functionality of existing AIL SLO technology with HTS

chirp filters. The authors acknowledge additional discussions with John Cafarella, James Roberge, Leonard Johnson, Klaus Breuer, Stanley Reible, Richard Withers, James Tsui, Paul Ryan, Joseph Caschera, and Frank Elmer. The authors also express their gratitude to Earle Macedo and Daniel Baker for assistance in the fabrication of the HTS chirp filters described here, George Fitch for computer programming and chirp-filter lithography mask layout, John King for assistance in thin-film growth, Brian Reynolds and Terence Weir for their work in layout and space-qualified soldering of the complex circuit boards used in HTSSE, William Brogan for help with hermetic package preparation, Edward Mencow and John Connelly for their assistance in shock- and vibration-testing the HTSSE hardware, Jon Howell for help in thermal-vacuum-testing the HTSSE hardware, Robert Konieczka for expert work on the chirp-filter packaging, and Allen Pillsbury for consultation on space-qualified packaging. The staff at Assurance Technology Corporation provided effective screening and qualification of many of the commercially available receiver components. Woody Ewan, Martin Nisenoff, and George Price of the NRL have provided the excellent guidance and support required to qualify our HTSSE experiment for a space environment. Additional interactions with Scott Chappie, Vince Rose, Gerry Golba, Tom Kawecki, and Jeff Pond of NRL are appreciated. We also acknowledge the continued support of Stu Wolf and Frank Patten at DARPA.

REFERENCES

1. N. Newman and W.G. Lyons, "High-Temperature Superconducting Microwave Devices: Fundamental Issues in Materials, Physics, and Engineering," *J. Supercond.*, vol. 6, no. 3, pp. 119–160 (1993). This article contains a comprehensive review of interdisciplinary progress in HTS microwave devices through mid-1993.
2. Z.-Y. Shen, *High-Temperature Superconducting Microwave Circuits* (Artech, Boston, MA, 1994).
3. H.J. Chaloupka, M.A. Hein, and G. Muller, "HTS Microwave Applications in Europe," *SPIE*, vol. 2156, pp. 36–54 (1994).
4. J. Clarke, private communication; W.J. Gallagher, private communication.
5. R.G. Ross, *Cryocoolers 8* (Plenum, New York, 1995).
6. K.D. Breuer, J.S. Levy, and H.C. Paczkowski, "The Compressive Receiver: A Versatile Tool for EW Systems," *Microw. J.*, vol. 32, no. 10, pp. 81–98 (1989).
7. G.W. Anderson, D.C. Webb, A.E. Spezio, and J.N. Lee, "Advanced Channelization Technology for RF, Microwave, and Millimeterwave Applications," *Proc. IEEE*, vol. 79, no. 3, pp. 355–388 (1991).
8. J.B.-Y. Tsui, *Microwave Receivers with Electronic Warfare Applications* (Krieger, Malibu, FL, 1992).
9. G.S. Kino, *Acoustic Waves: Devices, Imaging, and Analog Signal Processing* (Prentice-Hall, Englewood Cliffs, NJ, 1987).
10. W.G. Lyons, D.R. Arsenault, A.C. Anderson, T.C.L.G. Sollner, P.G. Murphy, M.M. Seaver, R.R. Boisvert, R.L. Slattery, and R.W. Ralston, "High Temperature Superconductive Wideband Compressive Receivers," *IEEE Trans. Microw. Theory Tech.* vol. 44, no. 7, pp. 1258–1278 (1996).
11. J.T. Lynch, A.C. Anderson, R.S. Withers, P.V. Wright, and S.A. Reible, "Passive Superconducting Microwave Circuits for 2–20 GHz Bandwidth Analog Signal Processing," *1982 IEEE MTT-S Int. Microw. Symp. Dig.*, *Dallas, 15–17 June 1982,* pp. 524–526.
12. J.T. Lynch, R.S. Withers, A.C. Anderson, P.V. Wright, and S.A. Reible, "Multigigahertz-Bandwidth Linear-Frequency-Modulated Filters Using a Superconductive Stripline," *Appl. Phys. Lett.*, vol. 43, no. 3, pp. 319–321 (1983).
13. S.A. Reible, "Wideband Analog Signal Processing with Superconductive Circuits," *Proc. 1982 IEEE Ultrasonics Symp.*, *Vol. 1*, *San Diego, 27–29 Oct. 1982*, pp. 190–201.
14. R.S. Withers, A.C. Anderson, J.B. Green, and S.A. Reible, "Superconductive Delay-Line Technology and Applications," *IEEE Trans. Magn.*, vol. 21, no. 2, pp. 186–192 (1985).
15. R.S. Withers and R.W. Ralston, "Superconductive Analog Signal Processing Devices," *Proc. IEEE*, vol. 77, no. 8, pp. 1247–1263 (1989).
16. R.S. Withers and P.V. Wright, "Superconductive Tapped Delay Lines for Low-Insertion-Loss Wideband Signal-Processing Filters," *Proc. 37th Annual Frequency Control Symp.*, *Philadelphia, 1–3 June 1983,* pp. 81–86; F. Huang, "Quasi-Transversal Synthesis of Microwave Chirped Filters," *Electron. Lett.*, vol. 28, no. 11, pp. 1062–1064 (1992).
17. R. Ramisch, G.R. Olbrich, and P. Russer, "A Tapped-Delay-Line Superconductive Chirp Filter in Shielded Microstrip," *IEEE Trans. Microw. Theory Tech.*, vol. 39, no. 9, pp. 1575–1581 (1991).
18. R.S. Withers and S.A. Reible, "Superconductive Chirp-Transform Spectrum Analyzer," *IEEE Electron Device Lett.*, vol. 6, no. 6, pp. 261–263 (1985).

19. M.S. DiIorio, R.S. Withers, and A.C. Anderson, "Wide-Band Superconductive Chirp Filters," *IEEE Trans. Microw. Theory Tech.*, vol. 37, no. 4, pp. 706–710 (1989).
20. C.E. Cook and M. Bernfeld, *Radar Signals: An Introduction to Theory and Application* (Academic Press, New York, 1967).
21. W.G. Lyons, D.R. Arsenault, J.H. Holtham, R.W. Ralston, and T.C.L.G. Sollner, unpublished.
22. W.G. Lyons, R.S. Withers, J.M. Hamm, A.C. Anderson, P.M. Mankiewich, M.L. O'Malley, and R.E. Howard, "High-T_c Superconductive Delay Line Structures and Signal Conditioning Networks," *IEEE Trans. Magn.*, vol. 27, no. 2, pp. 2932–2935 (1991).
23. W.G. Lyons, R.S. Withers, J.M. Hamm, A.C. Anderson, P.M. Mankiewich, M.L. O'Malley, R.E. Howard, R.R. Bonetti, A.E. Williams, and N. Newman, "High-Temperature Superconductive Passive Microwave Devices," *1991 IEEE MTT-S Int. Microw. Symp. Dig., Vol. 3, Boston, 10–14 June 1991* pp. 1227–1230.
24. W.G. Lyons, R.S. Withers, J.M. Hamm, R.H. Mathews, B.J. Clifton, P.M. Mankiewich, M.L. O'Malley, and N. Newman, "High-Frequency Analog Signal Processing with High-Temperature Superconductors," *OSA Proc. on Picosecond and Optoelectronics, Vol. 9, Salt Lake City, 13–15 Mar. 1991,* pp. 167–173 (1991).
25. W.G. Lyons, R.S. Withers, J.M. Hamm, A.C. Anderson, D.E. Oates, P. M. Mankiewich, M.L. O'Malley, R.R. Bonetti, A.E. Williams, and N. Newman, "High-Temperature Superconductive Delay Lines and Filters," in *Superconductivity and Its Applications, Vol. 251* (American Institute of Physics, New York, 1992), pp. 639–658.
26. N. Fenzi, D. Aidnik, D. Skoglund, and S. Rohlfing, "Development of High Temperature Superconducting 100 Nanosecond Delay Line," *SPIE,* vol. 2156, pp. 143–151 (1994).
27. W.G. Lyons and R.S. Withers, "Passive Microwave Device Applications of High-T_c Superconducting Thin Films," *Microw. J.*, vol. 33, no. 11, pp. 85–102 (1990).
28. G.C. Liang, R.S. Withers, B.F. Cole, S.M. Garrison, M.E. Johansson, W.S. Ruby, and W.G. Lyons, "High-Temperature Superconducting Delay Lines and Filters on Sapphire and Thinned $LaAlO_3$ Substrates," *IEEE Trans. Appl. Supercond.*, vol. 3, no. 3, pp. 3037–3042 (1993).
29. W.D. White, "Signal Translation Apparatus Utilizing Dispersive Network and the Like, for Panoramic Reception, Amplitude-Controlling Frequency Response, Signal Frequency Gating, Frequency-Time Conversion, Etc.," U.S. Patent 2,954,465 (27 Sept. 1960).
30. W.E. Morrow, J. Max, J. Petriceks, and D. Karp, "A Real-Time Fourier Transformer," *Group 36 Report*, MIT Lincoln Laboratory (16 July 1963), DTIC# AD-413786; R.M. Lerner, "Impulse Noise Suppression Communication System Utilizing Matched Filters and Noise Clipping," U.S. Patent 3,252,093, filed 9 Oct. 1961 and issued 17 May 1966.
31. D.C. Schleher, *Introduction to Electronic Warfare* (Artech, Dedham, MA, 1986).
32. M.A. Jack, P.M. Grant, and J.H. Collins, "The Theory, Design, and Application of Surface Acoustic Wave Fourier-Transform Processors," *Proc. IEEE,* vol. 68, no. 4, pp. 450–468 (1980).
33. M.A. Jack and E.G.S. Paige, "Fourier Transformation Processors Based on Surface Acoustic Wave Chirp Filters," *Wave Electron.*, vol. 3, no. 3, pp. 229–247 (1978).
34. J.B.G. Roberts, G.L. Moule, and G. Parry, "Design and Application of Real-Time Spectrum-Analyser Systems," *IEE Proc.*, vol. 127, pt. F, no. 2, pp. 76–91 (1980).
35. C. Campbell, *Surface Acoustic Wave Devices and Their Signal Processing Applications* (Academic Press, Boston, 1989).
36. D.P. Morgan, *Surface-Wave Devices for Signal Processing* (Elsevier, Amsterdam, 1985).
37. K.D. Breuer, J.J. Whelehan, and K. Ross, "Compressive Receivers Applied to ESM System Design," *Microw. Syst. News*, vol. 16, no. 10, pp. 66–75 (1986).
38. M.I. Skolnik, *Radar Handbook* (McGraw-Hill, New York, 1990).
39. M.D. Koontz, "Miniature Acousto-Optic Module Fabrication," *SPIE*, vol. 2489, pp. 89–94 (1995).
40. T.G. Kawecki, G.A Golba, G.E. Price, V.S. Rose, and W. Meyers, "The High Temperature Superconductivity Space Experiment (HTSSE-II) Design," *IEEE Trans. Microw. Theory Tech.,* vol. 44, no. 7, pp. 1198–1212 (1996). This article and Reference 10 appear as part of a special issue of *IEEE Transactions on Microwave Theory and Techniques,* which focuses on microwave HTS applications, particularly NRL's HTSSE program. The special-issue guest editorial contains additional background information on HTSSE.
41. M. Nisenoff, J.C. Ritter, G. Price, and S.A. Wolf, "The High Temperature Superconductivity Space Experiment: HTSSE I—Components and HTSSE II—Subsystems and Advanced Devices," *IEEE Trans. Appl. Supercond.*, vol. 3, no. 1, pp. 2885–2890 (1993).
42. T.C.L.G. Sollner, W.G. Lyons, D.R. Arsenault, A.C. Anderson, M.M. Seaver, R.R. Boisvert, and R.L. Slattery, "Superconducting Cueing Receiver for Space Experiment," *IEEE Trans. Appl. Supercond.*, vol. 5, no. 2, pp. 2071–2074 (1995).
43. W.G. Lyons, D.R. Arsenault, M.M. Seaver, R.R. Boisvert, T.C.L.G. Sollner, and R.S. Withers, "Implementation of a $YBa_2Cu_3O_{7-x}$ Wideband Real-Time Spectrum-Analysis Receiver," *IEEE Trans. Appl. Supercond.*, vol. 3, no. 1, pp. 2891–2894 (1993).
44. W.G. Lyons, M.M. Seaver, D.R. Arsenault, R.R. Boisvert, and T.C.L.G. Sollner, "Demonstration of a 3-GHz-Bandwidth Real-Time Spectral-Analysis Receiver Based on a High-T_c Superconductive Chirp Filter," *Microw. Opt. Technol. Lett.*, vol. 6, no. 13, pp. 728–732 (1993); errata, *Microw. Opt. Technol. Lett.*, vol. 7, no. 18, p. 875 (1994).
45. A.D. Pillsbury, private communication.
46. W.G. Lyons, R.R. Bonetti, A.E. Williams, P.M. Mankiewich, M.L. O'Malley, J.M. Hamm, A.C. Anderson, R.S. Withers, A. Meulenberg, and R.E. Howard, "High-T_c Superconductive Microwave Filters," *IEEE Trans. Magn.*, vol. 27, no. 2, pp. 2537–2539 (1991).
47. A.C. Westerheim, L.S. Yu-Jahnes, and A.C. Anderson, "Off-Axis Magnetron Sputtering of YBCO Films: The Influence of Atomic Oxygen," *IEEE Trans. Magn.*, vol. 27, no. 2, pp. 1001–1005 (1991).
48. A.C. Anderson, R.L. Slattery, D.E. Oates, and L.S. Yu-Jahnes, "Cylindrical Magnetron Deposition of High-Quality High-Temperature Superconductive Thin Films," *Solid State Research Report 1993:2,* MIT Lincoln Laboratory (15 May 1993), DTIC #AD-A274063.
49. W.G. Lyons, D. Barry, R. Guadagnolo, P.G. Murphy, R.R. Boisvert, A.C. Anderson, M.M. Seaver, D.R. Arsenault, R.L. Slattery, D.J. Baker, E.M. Macedo, and G.L. Fitch, "Lincoln/Hughes Compressive Receiver Demonstration with 24-nsec Bonded-Wafer $YBa_2Cu_3O_{7-\delta}$ Chirp Filters," *Solid State Research Report 1995:1,* MIT Lincoln Laboratory (15 Feb. 1995), DTIC #AD-A298813.
50. W.G. Lyons, P.G. Murphy, R.R. Boisvert, A.C. Anderson, D.R. Arsenault, M.M. Seaver, R.W. Ralston, and T.C.L.G.

Sollner, "Demonstration of a 40-nsec $YBa_2Cu_3O_{7-\delta}$ Chirp Filter on 125-μm Bonded-Wafer $LaAlO_3$ Substrates," *Solid State Research Report, 1995:3,* MIT Lincoln Laboratory (15 Aug. 1995), DTIC #AD-A311816.

51. R.W. Klopfenstein, "A Transmission-Line Taper of Improved Design," *Proc. IRE*, vol. 44, no. 1, pp. 31–35 (1956).
52. P.J. Burke, "Ultra-Linear Chirp Generation via VCO Tuning Predistortion," *1994 IEEE MTT-S Int. Microw. Symp. Dig., Vol. 2, San Diego, 23–27 May 1994,* pp. 957–960.
53. J. Levy, P.J. Burke, L.D. Cohen, and R. Cecchini, "VCO Based Chirp Generation for Broad Bandwidth Compressive Receiver Applications," *1993 IEEE MTT-S Int. Microw. Symp. Dig., Vol. 2, Atlanta, 14–18 June 1993,* pp. 1113–1115.
54. J. Levy, private communication.
55. L.D. Cohen and K. Breuer, "A Fast-Tuned, Injection-Locked, DDS-Based Local Oscillator for the 3.6 to 4.1 GHz Frequency Range," *1993 IEEE MTT-S Int. Microw. Symp. Dig., Vol. 2, Atlanta, 14–18 June 1993,* pp. 659–662.
56. M.W. Pospieszalski, S. Weinreb, R.D. Norrod, and R. Harris, "FET's and HEMT's at Cryogenic Temperatures—Their Properties and Use in Low-Noise Amplifiers," *IEEE Trans. Microw. Theory Tech.*, vol. 36, no. 3, pp. 552–560 (1988); S. Weinreb, D.L. Fenstermacher, and R.W. Harris, "Ultra-Low-Noise 1.2- to 1.7-GHz Cooled GaAsFET Amplifiers," *IEEE Trans. Microw. Theory Tech.*, vol. 30, no. 6, pp. 849–853 (1982).
57. J.B. Barner, J.J. Bautista, J.G. Bowen, W. Chew, M.C. Foote, B.H. Fujiwara, A.J. Guern, B.J. Hunt, H.H.S. Javadi, G.G. Ortiz, D.L. Rascoe, R.P. Vasquez, P.D. Wamhof, K.B. Bhasin, R.F. Leonard, R.R. Romanofsky, and C.M. Chorey, "Design and Performance of Low-Noise, Hybrid Superconductor/Semiconductor 7.4 GHz Receiver Downconverter," *IEEE Trans. Appl. Supercond.*, vol. 5, no. 2, pp. 2075–2078 (1995).
58. G.-C. Liang, C.-F. Shih, R.S. Withers, B.F. Cole, M.E. Johansson, and L.P. Suppan, "Superconductive Digital Instantaneous Frequency Measurement Subsystem," *IEEE Trans. Microw. Theory Tech.*, vol. 41, no. 12, pp. 2368–2375 (1993).
59. Z.-Y. Shen, C. Wilker, P.S.W. Pang, C.F. Carter III, V.X. Nguyen, and D.B. Laubacher, "High-Temperature Superconductor/III-V Hybrid Microwave Circuits," *Microw. Opt. Technol. Lett.*, vol. 6, no. 13, pp. 732–736 (1993).
60. N. Fenzi, K. Raihn, E. Soares, and G. Mathaei, "Development of an Optically Switched High-Temperature Superconducting Multichannel Bandstop Filter Bank," *SPIE*, vol. 2156, pp. 60–68 (1994).
61. D.C. DeGroot, J.A. Beall, R.B. Marks, and D.A. Rudman, "Microwave Properties of Voltage-Tunable $YBa_2Cu_3O_{7-\delta}$/$SrTiO_3$ Coplanar Waveguide Transmission Lines," *IEEE Trans. Appl. Supercond.*, vol. 5, no. 2, pp. 2272–2275 (1995).
62. D. Galt, J.C. Price, J.A. Beall, and T.E. Harvey, "Ferroelectric Thin Film Characterization Using Superconducting Microstrip Resonators," *IEEE Trans. Appl. Supercond.*, vol. 5, no. 2, pp. 2575–2578 (1995).
63. R.J. Forse and S. Rohlfing, "35 GHz Downconverter Using High-Temperature Superconductor Films," *SPIE*, vol. 2156, pp. 80–87 (1994).
64. S.H. Talisa, M.A. Janocko, D.L. Meier, C. Moskowitz, R.L. Grassel, J. Talvacchio, P. LePage, D.C. Buck, R.S. Nye, S.J. Pieseski, and G.R. Wagner, "High-Temperature Superconducting Wide Band Delay Lines,"*IEEE Trans. Appl. Supercond.*, vol. 5, no. 2, pp. 2291–2294 (1995).
65. K. Poulton, K.L. Knudsen, J.J. Corcoran, K.-C. Wang, R.B. Nubling, R.L. Pierson, M.C.F. Chang, P.M. Asbeck, and R.T. Huang, "A 6-b, 4 GSa/s GaAs HBT ADC," *IEEE J. Solid-State Circuits*, vol. 30, no. 10, pp. 1109–1118 (1995).
66. R.B. Nubling, J. Yu, K.C. Wang, P.M. Asbeck, N.H. Sheng, M.F. Chang, R.L. Pierson, G.J. Sullivan, M.A. McDonald, A.J. Price, and D.M. Chen, "High Speed 8:1 Multiplexer and 1:8 Demultiplexer Implemented with AlGaAs/GaAs HBTs," *1990 GaAs IC Symp. Tech. Dig., New Orleans, 7–10 Oct. 1990,* pp. 53–56.
67. M. Fujishima, K. Asada, Y. Omura, and K. Izumi, "Low-Power 1/2 Frequency Dividers Using 0.1-μm CMOS Circuits Built with Ultrathin SIMOX Substrates," *IEEE J. Solid-State Circuits*, vol. 28, no. 4, pp. 510–512 (1993).
68. Y. Kado, M. Suzuki, K. Koike, Y. Omura, and K. Izumi, "A 1-GHz/0.9-mW CMOS/SIMOX Divide-by-128/129 Dual-Modulus Prescaler Using a Divide-by-2/3 Synchronous Counter," *IEEE J. Solid-State Circuits*, vol. 28, no. 4, pp. 513–517 (1993).
69. L. Peters, "SOI Takes Over Where Silicon Leaves Off," *Semiconductor Int.*, pp. 48–51 (Mar. 1993).
70. R.P. Baker and J.H. Cafarella, "Hybrid Convolver Signal Processor Achieves High Processing Gain," *1980 IEEE Ultrasonics Symp., Vol. 1, New York, 5–7 Nov. 1980,* pp. 5–9.
71. J.H. Fischer, J.H. Cafarella, D.R. Arsenault, G.T. Flynn, and C.A. Bouman, "Wide-Band Packet Radio Technology," *Proc. IEEE*, vol. 75, no. 1, pp. 100–115 (1987).
72. M.I. Skolnik, *Introduction to Radar Systems* (McGraw-Hill, New York, 1980).
73. C.D. McGillem and G.R. Cooper, *Continuous and Discrete Signal and System Analysis* (Holt, Rinehart, and Winston, New York, 1974).
74. I.H. Gilbert and W.S. Farmer, "The Mesh Synchronous Processor MeshSP," *Technical Report 1004,* MIT Lincoln Laboratory (14 Dec. 1994), DTIC #AD-A289875.
75. J.H. Cafarella, "Wideband Signal Processing for Communication and Radar," *Proc. 1983 IEEE National Telesystems Conf., San Francisco, 14–16 Nov. 1983,* pp. 55–58.
76. John Przybysz, private communication.
77. P. Singer, "1995: Looking down the Road to Quarter-Micron Production," *Semicond. Int.*, pp. 46–52 (Jan. 1995).